Ocean Systems Engineering, *Vol. 15, No. 1 (2025) 91-125*
https://doi.org/10.12989/ose.2025.15.1.091

Design and development of a finite element analysis based model for impact analysis of blasts incorporating material properties

Pankaj Meena[a] and R. Sharma[*]

Design and Simulation Laboratory, Department of Ocean Engineering, IIT Madras, Chennai (TN) - 600036, India

(Received October 27, 2024, Revised February 20, 2025, Accepted February 25, 2025)

Abstract. Herein, we present the design and development of a 'Finite Element Analysis (FEA)' based model incorporating temperature dependent material properties for impact analysis of blasts on underwater vehicles. Our primary idea is the incorporation of temperature dependent material properties in explosion studies for the design and development of new age shield engineering designs, especially focused towards the applications relevant to the underwater vehicles (e.g. autonomous underwater vehicles, submarines, submersibles, and torpedoes, etc.). We present extensive results that are key towards bench marking. Furthermore, we show and analyse the effect of explosion on square plates of different materials and distribution of stresses, strains and displacements after explosion/impact, etc., are examined in-detail. Our proposed FEA based model is governed by the basic numerical analysis, finite element analysis and thermal/material science. We implement our model in ABAQUS[*TM] and Matlab[**TM] software solution systems and develop subroutines to ensure seamless integration. In our model the focus is on large deformation finite element analysis, and we use the Jones-Wilkins-Lee (JWL) equation of state, Johnson Cook parameters, along with temperature dependent material properties. Presented results examine the role of explosion at various heights in the z axis direction on plates of different materials and the '2, 4, 6-Tri Nitro Toluene (TNT)' is used as a representative explosive material. Finally, based upon the results and their analyses suitable design guidelines related to material selection and applications are derived.

Keywords: explosion; finite element analysis; impact analysis; large deformation analysis; material properties; temperature dependent material properties

1. Introduction

A blast load is the force exerted on a structure or object by a blast wave, and it is characterized by an overpressure and impulse or duration. In cases of uncontrolled explosions, such as 'Improvised Explosive Devices (IEDs), the load is determined by the explosive's type and payload weight. When high explosives detonate Fordham (2013), a blast wave is generated, impacting the structure with incident overpressure (P_{so}), Beshara (1994).

This wave is then reflected back as reflected excess pressure (PCa), Remennikov (2003),

∗Corresponding author, Professor, E-mail: rajivatri@zmail.iitm.ac.in
[a]Research Scholar, E-mail: pankajmn926@gmail.com

 ISSN: 2093-6702 (Print), 2093-677X (Online)

Mubarok *et al*. (2022). In the past, research on how the geometric structure of a plate responds to impact and various active loads including air blast loading, has been conducted, for details see Prabowo *et al*. (2019), Smaradhana *et al*. (2021). Explosive loading from landmines and improvised explosive devices (IEDs) pose significant threat to civil and defence underwater vehicles and infrastructure. Normally, steel and composite plates are used in various lightweight military assets, e.g. in armored vehicles, tanks, ships, submarines, aircraft, helicopters, and drones. And, these are at risk from explosive ammunitions. Metals can absorb a lot of shock wave energy by deforming before failing and because of this reason they have high ductility in comparison with composites, for details see Nurick *et al*. (1989), Rajendran and Lee (2009). Utilizing this property of high ductility, normally, naval ships and defense platforms, are built with steel. However, because of their extremely high compressive yield strength and low density, etc., the composite materials like glass fiber, and e-fiber, etc., have some specific applications in underwater vehicles, ships and other marine structures. An optimal choice of material depends on various design factors, including loading, manufacturing and assembly costs, operational life, maintenance costs, radar-absorbing properties, and magnetic signature, etc. Underwater vehicles, ships and other marine structures face threats from underwater weapons like sea mines and torpedoes, as well as air weapons like missiles. The ability of these structures to resist large deformations, damage and failure is crucial for their survival. Some studies exist on the effect of air blast on steel plates, e.g., Nurick *et al*. (1989), Fu *et al*. (2021), however these studies have focused only upon plates of low thicknesses (less than or equal to 10 mm). In general, within the context of marine structures, only limited research results exist on the deformation and failure of marine-grade steel and glass fibers subjected to the impact through explosion. We note that the resistance of steel, aluminium alloy, and composites depend on various material properties, such as Young's modulus, yield stress, dynamic strain hardening rate, Poisson's ratio, and strain failure rate etc., and additionally, also it is influenced by geometric parameters, including the thickness, aspect ratio, and shape of the target plate, and as well as boundary conditions, etc.

Furthermore, the characteristics of the explosive charge, such as the type of explosive material, its mass, stand-off distance, and the medium (air, water, and multiphases of air and water), influence the behavior of plates under impact through explosion. As both the metals and composites are used in the underwater vehicles and marine structures, it is important to analyses the behavior of plates of both metals and composites under impact through explosion, with different characteristics of the explosive charges. This requirement has motivated our present work.

Herein, we present the design and development of a 'Finite Element Analysis (FEA)' based model incorporating temperature dependent material properties for impact analysis of blasts on underwater vehicles. We incorporate temperature dependent material properties in impact through explosion studies for the design and development of new age shield engineering designs, and we focus towards the applications relevant to the underwater vehicles (e.g., autonomous underwater vehicles, submarines, submersibles, and torpedoes, etc.). Utilizing the proposed FEA based model, we report extensive results that are key towards bench marking and show and analyse the effect of explosion on square plates of different materials and distribution of stresses, strains and displacements after explosion/impact, etc., are examined in-detail. Our proposed FEA based model is governed by the basic numerical analysis, finite element analysis and thermal/material science. We implement our model in ABAQUS^{*TM} and Matlab^{**TM} software solution systems and develop subroutines to ensure seamless integration. In our model the focus is on large deformation finite element analysis, and we use the Jones-Wilkins-Lee (JWL) equation of state, Johnson Cook

parameters, along with temperature dependent material properties. Reported results examine the role of explosion at various heights in the z axis direction on plates of different materials and the '2, 4, 6-Tri Nitro Toluene (TNT)' is used as a representative explosive material.

1.1 Motivation

Necessity of the modern marine structures to with stand the impact through explosion has motivated our research. Our aim is to ensure that an efficient FEA based model exists and it can be utilized to analyze both the metal and composite plates to be used in the underwater vehicles and marine structures.

1.2 Objective and scope

Objective is to design and develop a FEA based model to study the impact through explosion for analyzing both the metal and composite plates. Through this FEA based model, we compute and evaluate different relevant parameter for analysis and design, e.g., deformations, stresses, strains, etc. Scope of our research includes square plates of steel and e-glass fiber with different thicknesses; and the blasts of different masses and at different locations, etc.

2. Brief review of literature

When an explosion happens, it creates a shock wave that impacts different materials in complex ways. How the shock wave affects something depends on the factors like the size and shape of the explosive, how close the explosion is, and the shape and material of the object being hit, for more details see Cole and Weller (1948), and Shi *et al*. (2007). Detonation of an explosive charge produces a localized region of highly compressed, hot gas that expands rapidly. Once the explosive reaction process starts, a detonation wave moves through the unreacted explosive material at a speed of approximately 6 to 8 km/s, and this process transforms the solid explosive material into a hot, high-pressure gas with a transient maximum temperature of approximately 3000°C and peak pressure reaching up to 40 GPa, Cimpoeru *et al*. (2017). Due to the high pressure, the gaseous detonation products expand rapidly to approximately 4000 times the original volume of the explosive charge. This rapid gas expansion almost instantaneously compresses the surrounding air or water into a shock wave, and this is known as a blast wave. A shock wave is a high-pressure compressive wave that travels through air, water, or another medium at a velocity faster than the speed of sound and a distinctive feature of a blast wave propagating in the air is that the shock front causes a nearly instantaneous step change in all gas dynamic conditions, including static pressure, density, flow velocity, and temperature, Cimpoeru *et al*. (2017). An air shock wave causes a sudden spike in pressure followed by a rapid decline, and this affects the characteristics of the blast load in air. These are shown in Fig. 1. When the explosive charge detonates, it generates a high-intensity shock wave by compressing the surrounding air and upon reaching the exposed surfaces at the arrival time (t_a), this shock wave abruptly raises the pressure from the ambient level to the peak pressure (P_P). Following this peak, the pressure exponentially decreases back to atmospheric pressure (P_{atm}) over the decay time duration (t_d), then drops further to a negative pressure (P_N), and eventually returns to the local ambient pressure at time $t_a + t_d + t_d\hat{}$. Positive pressure phase is represented above the P_{atm} line until the end of the positive phase duration (t_d),

after which the negative or suction phase occurs below the P_{atm} line, lasting up to the time duration of t_{d^-} in the air blast pressure profile, Kumar and Patel (2021). Free-field air blast wave is characterized with the help of the modified Friedlander Equation. Characteristics of a blast wave primarily depend on the source or material of the explosion, the mass of the explosive charge, and the stand-off distance. From Fig. 1, we note that the effects of the blast wave in the negative pressure zone are often disregarded in most of the blast studies mainly because the primary damage is typically caused by the positive pressure zone. Therefore, only the positive pressure zone is normally considered in most of the analyses, Dharmasena *et al.* (2008). Also, from Fig. 1, we note that the positive overpressure decays exponentially with time. Utilizing the basics of impact mechanics, some researchers have investigated the analysis of impact (through explosion) on marine structures, e.g. Hamdoon *et al.* (2011), Shin (2011), Kim *et al.* (2015), Das *et al.* (2022). Overall, cautiously, we can note that although, significant research exists on the mechanics of impact through explosion, literature on the studies related to metals and composites with the reference to material properties, and the characteristics of the explosive charge, is rare. This remains largely unexplored. Our present work is an effort to fill this gap.

3. Basics and the governing equations of the FEA based model

Following Mohamed (2023), Xu *et al*. (2020) and Patel *et al.* (2023), the relation between '*p–t*' responses is defined by a modified Friedlander equation, i.e.

$$P(t) = (P_P - P_{atm})\left[1 - \frac{t-t_\alpha}{t_d}\right] e^{-(t-t_a)/\lambda} \tag{1}$$

where P (t) is the instantaneous overpressure at time t, P_P is the peak overpressure when t is zero (i.e., t_a is the arrival time of the wave front), t_d is the time duration after the wave front, P_{atm} is the atmospheric pressure, and λ is the time decay constant. Following Mohamed (2023), the relation between instantaneous overpressure (P) with reference to the mass and distance of a given explosive is

$$P = K\left[\frac{m}{R^3}\right] \tag{2}$$

where K is the explosive material constant, m is the explosive mass, and R is the stand-off distance. Using Eq. (1), we obtain the imparted impulse (I) by integrating the pressure acting with respect to the time duration of the loading and it is

$$I = \int_{t_a}^{t_a+t_d} p\, dt \tag{3}$$

where p represents the applied pressure due to the blast loading function and other parameters are the same, as defined before. Following Mouritz (2019), for a far-field explosion, we describe the peak overpressure by

$$P_p \approx 53.9\left(\frac{W^{0.33}}{R}\right)^{1.13} \tag{4}$$

where W is the weight and R is the stand-off distance of the explosive charge (same as defined in Eq. (2)).

As the shock wave propagates away from the original location of the explosive charge, its pressure amplitude decreases. Over expansion at the blast source's center creates a vacuum, resulting in high suction and a reversal of particle motion. This phenomenon produces a negative pressure below ambient levels following the initial positive pressure phase. Negative phase generally lasts longer than the positive phase but it has a significantly lower amplitude. Overall, positive phase loads are far more damaging to materials and structures than negative phase loads, Mlakar and Barker (2010). Air shock waves can produce extremely high impulse pressures over very short durations, typically within 0.01 to 1 second, depending on the mass and stand-off distance of the explosive charge. When an air blast wave impacts a structure, it subjects the structure to high pressures at high strain rates, generally between approximately 100 and 10,000 s^{-1}. This can result in severe dynamic deformation, vibrations, and structural damage. We consider the same in our work here.

3.1 Governing equations for the materials and their mechanics

For the materials and their mechanics related simulation and analysis, we use the basic formulations available from fluid-structure interaction under air blast loading. Following Kinney and Graham (2013), Longère *et al.* (2013), and Markose and Rao (2017), we use an empirical equation to calculate the shock wave pressure exerted on a surface and the explosion generates a pressure wave, as shown in Fig. 1. Structural interactions are numerically modeled using this empirical equation and the mass of TNT is used to characterize the explosive charge. We compute the angle of incidence by integrating the reflected pressure (normal incidence) and the incident pressure (side-on incidence). Now, following Kinney and Graham (2013), Longère *et al.* (2013), Markose and Rao (2017), Yadav *et al.* (2020) and Mubarok *et al.* (2022a), we compute the scaled distance or the proximity factor (Z) in $m/kg^{1/3}$ using

$$Z = \frac{R}{m^{1/3}} \tag{5a}$$

and Eq. (5(a)) is related to Eq. (2) through:

$$Z = \frac{R}{m^{1/3}} = \left[\frac{K}{P}\right]^{1/3} \tag{5b}$$

where R is the stand-off distance, as defined before, and it refers to the distance from the center of the explosion to the target structure, and other parameters are the same as defined before. We note that the greater the stand-off distance, the less structural damage from the blast wave is expected. Then, the R is expressed

$$R = \sqrt{h^2 + x^2} \tag{6}$$

$$P_s = P_i(1 + cos\theta - 2cos^2\theta + P_r cos^2\theta) \tag{7}$$

where P_s is the shock wave overpressure, θ is the incident wave angle, and the P_i and P_r are the incident and reflected overpressures, respectively. For material characterization we use the standard Johnson-Cook model and adopt an elastoplastic material representation incorporating Johnson-Cook strain hardening and damage initiation. Following Mubarok *et al.* (2022b) and Yadav *et al*. (2020), the Johnson-Cook strain rate dependence is

$$\begin{aligned} \bar{\sigma} &= \sigma^0\left(\bar{\varepsilon}^p_{eq}, T\right)\varepsilon_R\left(\dot{\bar{\varepsilon}}^p_{eq}\right). \text{and} \\ \dot{\bar{\varepsilon}}^p_{eq} &= \dot{\varepsilon}_0 exp\left[\frac{1}{c}(\varepsilon_R - 1)\right] \; for \; \bar{\sigma} \geq \sigma^0 \end{aligned} \tag{8, 9}$$

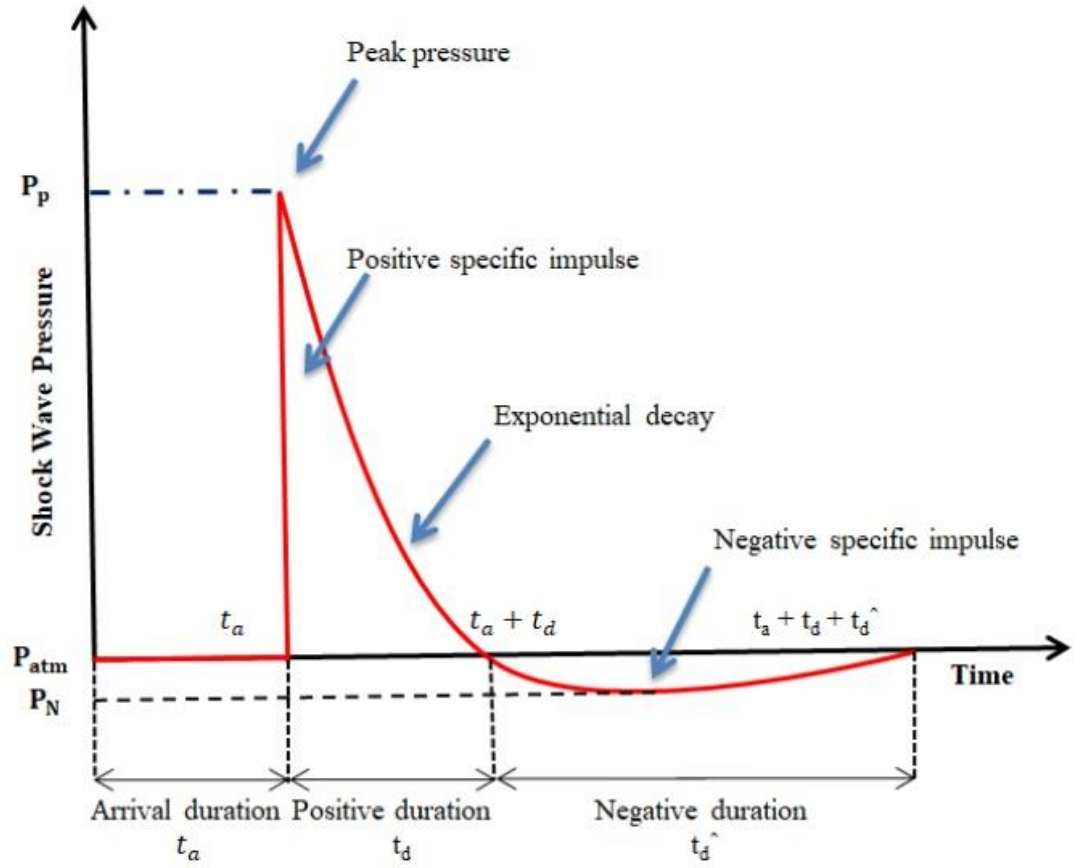

Fig. 1 Overpressure-time history of a shock wave generated by a far-field explosion adapted from Patel *et al.* (2023)

where $\bar{\sigma}$ is the yield stress at non-zero strain rate, $\bar{\varepsilon}_{eq}^{p}$ is the equivalent plastic strain rate, $\dot{\varepsilon}_0$ is the reference strain rate, $\sigma^0\left(\bar{\varepsilon}_{eq}^{p}, T\right)$ is the static yield stress, and $\varepsilon_R\left(\bar{\varepsilon}_{eq}^{p}\right)$ is the ratio of the yield stress at nonzero strain rate to the static yield stress. Equivalent Von-Mises yield stress is

$$\bar{\sigma} = \left(A_v + B_v\left(\bar{\varepsilon}_{eq}^{p}\right)^{n_v}\right)\left(1 + C_v ln_v\left(\frac{\bar{\varepsilon}_{eq}^{p}}{\dot{\varepsilon}_0}\right)\right)\left(1 - (T^*)^{m_v}\right) \tag{10}$$

where A_v, B_v, n_v, C_v, and m_v are material parameters, and T^* is expressed

$$T^* = \begin{cases} 0, & for\ T < T_r, \\ \frac{T - T_r}{T_m - T_r} & for\ T_r \le T \le T_m \\ 1, & for\ T > T_m, \end{cases} \tag{11}$$

where T is the material temperature, T_m is the melting temperature of the material, and T_r is the room temperature, i.e. all the temperatures are in degree Kelvin. For the damage initiation and

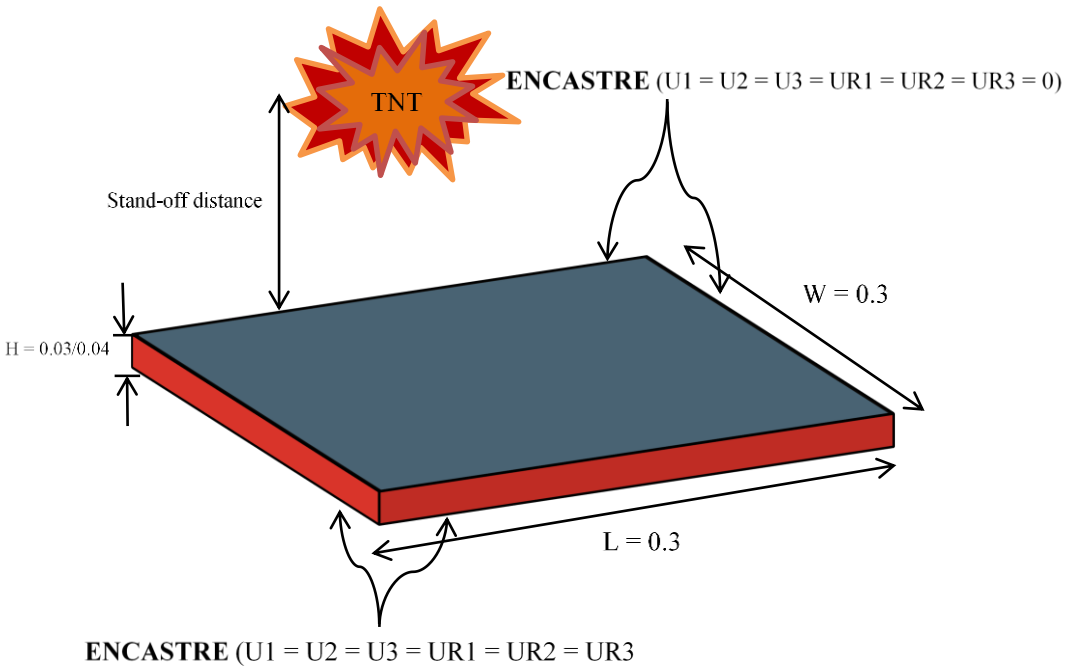

Fig. 2 Basic schematic, convention and plate modeling features

evolution, we use the Johnson-Cook method, and following Johnson and Cook (1985), the damage is based on the value assumed by a variable D, and it is defined

$$D = \sum \frac{\Delta_\varepsilon}{\varepsilon^f} \tag{12}$$

where Δ_ε is the equivalent plastic strain and ε^f is the equivalent strain required to fracture. We note that the fracture will occur when $D \geq 1$. Following Johnson and Cook (1985) and Iqbal *et al.* (2015), the general form of the equivalent strain required to fracture (ε^f) is:

$$\varepsilon^f = [D_1 + D_2 \exp\ D_3\sigma^*][1 + D_4 \ln\ \varepsilon^*][1 + D_5 T^*] \tag{13}$$

where σ^* is defined as $\sigma_m/\bar{\sigma}_v$ with σ_m denoting the average normal stresses and $\bar{\sigma}_v$ denoting the Von-Mises equivalent stress. The $D_1, D_2, D_3, D_4, and\ D_5$ are different fracture strain constants and these are primarily the material related parameters which are obtained experimentally. Herein, for each material case, we list them in Tables 1 and 2.

Although, our larger aim is to understand the impact mechanics of explosion through different mediums (i.e. air, water and combination of air and water), in this paper, we restrict and limit our formulation to the air medium only. We treat air as a non-viscous ideal gas with a linear polynomial equation and following Xu *et al.* (2020), the equation of state is

$$P_a = C_0 + C_1\mu + C_2\mu^2 + C_3\mu^3 + (C_4 + C_5\mu + C_6\mu^2)E_0 \tag{14}$$

where P_a is the air pressure, the μ is equal to V_0/V-1 (where V_0 is the initial relative volume, and V is the relative volume), the E_0 is the initial internal energy density, and C_0- C_6 are the coefficients

of the polynomial equation. And, the Jones - Wilkins - Lee (JWL) state equation is

$$P_d = A_j\left(1-\frac{\omega\rho_d}{R_1\rho_0}\right)\exp\left(-R_1\frac{\rho_0}{\rho_d}\right) + B_j\left(1-\frac{\omega\rho_d}{R_2\rho_0}\right)\exp\left(-R_2\frac{\rho_0}{\rho_d}\right)+\omega\rho_d E_m \tag{15}$$

where P_d is the detonation pressure, E_m is the internal energy per unit mass, ρ_0 is the density of the unreacted explosive material, ρ_d is the density of the reacted detonation products; and A_j, B_j, R_1, R_2 and ω are the material constants. Behavior of detonation products at very high pressures and intermediate pressure is, respectively, described by the first and second terms of the equation, Elek *et al.* (2015) and Giam *et al.* (2020).

We implement the model presented above in '**Section 3**' in a standard software solution system (i.e., ABAQUS*TM) and write the specific sub-routines for incorporating Eqs. (1)-(15) in to the FEA based model. Different material and cross sectional properties are modelled through the sub-routines developed in the Matlab**TM. Basic schematic, convention and plate modeling features are shown in Fig. 2. Overall, the flow chart followed in the designed and developed model is shown in Fig. 3(a).

3.2 Implementation details

Formulation presented in Section 3, is implemented while considering the time-dependent dynamic explicit solution and concentrated and distributed both types of explosions are modeled.

Table 1 List of the material properties of mild steel adapted from Iqbal *et al*. (2015)

Description	Notation	Numerical value
Density (kg/m³)	ρ	7850
Young's modulus (GPa)	E	203
Poisson's ratio	v	0.3
Yield stress (MPa)	σ_{YA}	304.33
Strain hardening constant (MPa)	B	422.007
Strain hardening coefficient (-)	n	0.345
Strain-rate hardening (-)	C	0.0156
Thermal softening constant (-)	m_t	0.87
Reference strain rate	ε_0	0.0001 s^{-1}
Melting temperature (in degree Kelvin)	T_m	1800
Transition temperature (in degree Kelvin)	T_t	293
Fracture strain constants (-) as defined in Equation (13)	D_1	0.1152
	D_2	1.0116
	D_3	-1.7684
	D_4	-0.05279
	D_5	0.5262

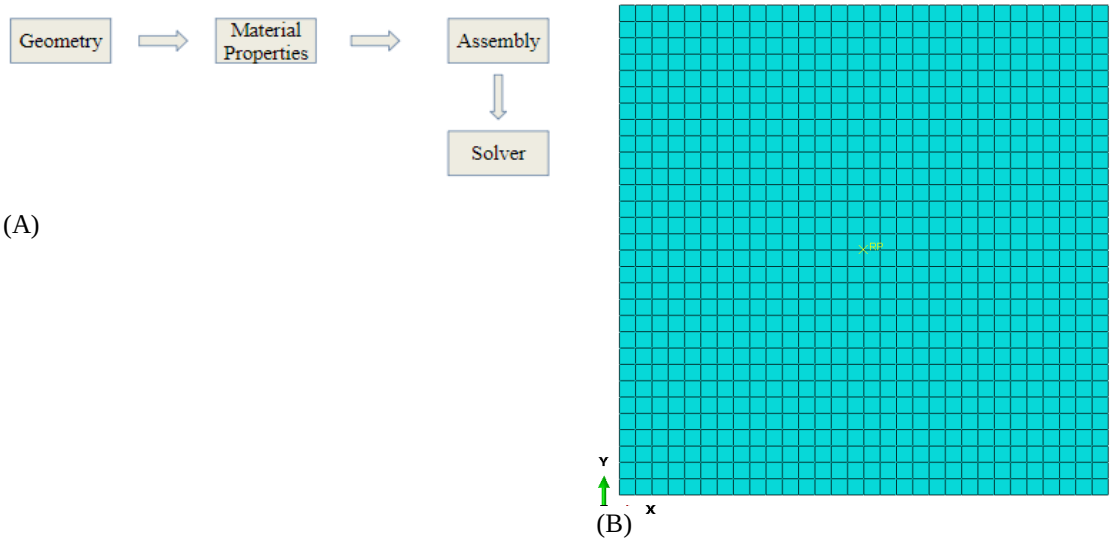

Fig. 3 (a) Basic flow chart followed in the designed and developed model and (b) Generated mesh of the plate)

Table 2 List of the material properties of e-glass fiber adapted from Shubham *et al*. (2022)

Description	Notation	Numerical value
Density (kg/m³)	ρ	2550
Young's modulus (GPa)	E	72
Poisson's ratio	v	0.23
Yield stress (MPa)	σ_{YA}	89.77
Strain hardening constant (MPa)	B	4200
Strain hardening coefficient (-)	n	1.4
Strain-rate hardening (-)	C	0.037
Thermal softening constant (-)	m_t	1
Reference strain rate	ε_0	0.0027 s^{-1}
Melting temperature (in degree Kelvin)	T_m	1725
Transition temperature (in degree Kelvin)	T_t	165
Fracture strain constants (-) as defined in Equation (13)	D_1	0.026
	D_2	0.05
	D_3	1.5
	D_4	0.028
	D_5	0.28

However, in this paper we present results of concentrated explosion, only. Our studies consider square plate in which two different types of plate materials along with two different thicknesses

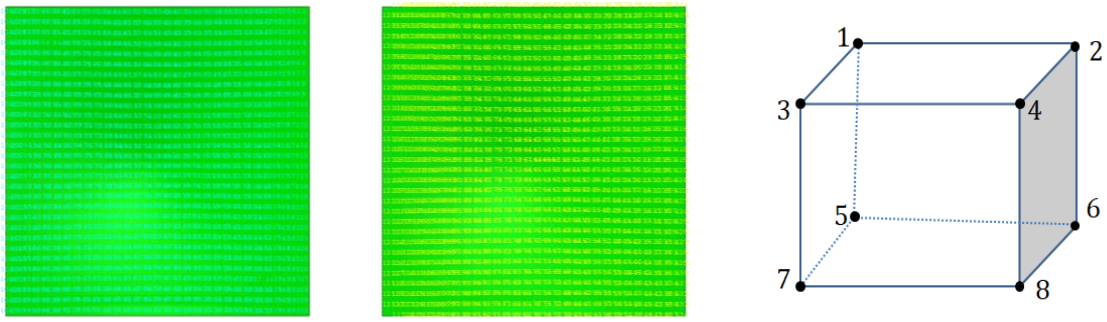

(a) (b) (c)

Fig. 4 (a) Elements' distribution of the plate, (b) Distribution of the nodes; and (c) Distribution of node number for 30/40 mm plate

are used for analysis and the plate is fixed from all the sides. We use explosive TNT for this analysis. Our analyses consider various heights of detonation from the plate in Z axis direction and the plate dimensions are: 0.3 m × 0.3 m and thicknesses of plate are 0.03 and 0.04 m. We consider two materials: Mild steel and e-glass fiber.

Different masses of the TNT are considered, i.e., 1 kg and 3 kg. Plate is modelled using 3D solid deformable extrusions and in the FEA model we consider: (i) 10800 elements and 12494 nodes for 30 mm plate, and (ii) 14400 elements and 16338 nodes for 40 mm plates in the presented examples. We arrive at these numbers of element and nodes through the process of mesh convergence study and these numbers are sufficient to ensure convergence and accuracy. We use the meshing available in ABAQUS^{*TM} and utilize the 'C3D8R (Element)'. This C3D8R is an eight noded linear brick element with reduced requirements of integration.

Elements' distribution of the plate, distribution of the nodes and distribution of node numbers are shown in Figs. 4 (a)-4(c), respectively, for the 30 mm thick plate. For the 40 mm plate it follows the same pattern, albeit with different numbers of the elements and nodes.

3.3 Details of the selected parameters and scaling

In our research, the scaled parameters have been determined from tests that were conducted in smaller scales, and these are used to predict the properties of large-scale explosions for various distances and energies. This approach is standard in impact mechanics research, e.g., Conrath (1999), Sachs (1944), and Ullah *et al.* (2017). Following them we note that the 'Hopkinson-Cranz (HC)' blast scaling law, in the form of cube root scaling, is the most commonly used blast scaling law, for more details see Hopkinson (1915), Cranz (1926). In the law, self-similar blast waves are produced at identically scaled distances by detonating two explosive charges of similar geometry and type but with different sizes in the same atmosphere. Following Mays and Smith (1995), Kim *et al.* (2009), Uddin (2010), and UNODA (2011), the scaled distance or the proximity factor (Z) in m/kg$^{1/3}$ is used as defined in Eq. (5(a)). We note that in-general the interpretation of small scale experimental data (e.g., 1 kg and 3 kg TNT explosions, etc.) for larger prototype structures typically involves dimensional analysis and blast scaling laws. Normally, the small scale tests with TNT charges are conducted at specific stand-off distances (e.g., 0.2, 0.3, 0.4, and 0.5, etc.), and then these results are interpolated/extrapolated to predict the behavior of larger prototype

Table 3 Relationship between model and prototype based upon scaling law as defined in Eq. (5(a))

Cases	**Stand-off distance (SoD) in m** **R_m = SoD for model, R_p = SoD for prototype**
Case I m_m (model) = 1 kg, m_p (prototype) = 5 kg	R_m = 0.0, 0.001, 0.1, 0.5, 2, 3.4. R_p = 0.0, 0.0017, 0.170, 0.850, 3.401, 5.782.
Case II m_m (model) = 1 kg, m_p (prototype) = 10 kg	R_m = 0.0, 0.001, 0.1, 0.5, 2, 3.4. R_p = 0.0, 0.0021, 0.213, 1.068, 4.275, 7.269.
Case III m_m (model) = 1 kg, m_p (prototype) = 15 kg	R_m = 0.0, 0.001, 0.1, 0.5, 2, 3.4. R_p = 0.0, 0.0024, 0.244, 1.222, 4.888, 8.309.
Case IV m_m (model) = 3 kg, m_p (prototype) = 5 kg	R_m = 0.0, 0.001, 0.1, 0.5, 2, 3.4. R_p = 0.0, 0.0011, 0.118, 0.591, 2.367, 4.024.
Case V m_m (model) = 3 kg, m_p (prototype) = 10 kg	R_m = 0.0, 0.001, 0.1, 0.5, 2, 3.4. R_p = 0.0, 0.0014, 0.148, 0.743, 2.975, 5.058.
Case VI m_m (model) = 3 kg, m_p (prototype) = 15 kg	R_m = 0.0, 0.001, 0.1, 0.5, 2, 3.4. R_p = 0.0, 0.0017, 0.170, 0.850, 3.401, 5.782.

structures by ensuring similarity in Z, e.g., if a full scale structure is designed to withstand 10 kg TNT explosion, then the stand-off distance R would be chosen to match the scaled distance Z of the smaller tests. This approach ensures the validity of numerical and experimental investigations across different scales while addressing practical constraints such as the computational feasibility and safety during experiments. In our work, different stand-off distances (e.g., 0.0 m, 0.001 m, 0.1 m, 0.5 m, 2 m, and 3.4 m) are used and these have been arrived based upon extensive review of literature, e.g., Safari *et al.* (2011), Aune *et al.* (2016), Li *et al.* (2017), and Gan *et al.* (2023). We list and analyze in Table 1 how these are related to the prototype for a blast of 5, 10 and 15 kg of TNT? These masses of TNT detonation are selected because of their importance in the real world applications, Gan *et al.* (2023), Patel and Patel (2024). From Table 3, we note that the mass of TNT detonation is inversely proportional to the stand-off distance and to study the effect of m_p mass of TNT explosion on prototype at R_p, for the model we need to consider m_m mass of TNT explosion at R_m, where $m_p > m_m$, and $R_m < R_p$.

To demonstrate the applicability and effectiveness of our developed model, we focus on plate thicknesses that are used in real world marine vehicles, i.e., 30 and 40 mm. For these thicknesses a low mass of TNT detonation is not sufficient to cause damage and our aim is to study the progressive impact of blast loading on the plate's performance and explore at what stand-off distance and mass of TNT detonation the plate will fail? Because of these reasons, we use 1 kg and 3 kg TNT masses as these allow desired analyses and help in proper understanding of deformation and damage mechanisms. Also, our selected TNT mass values represent controlled increments of blast energy to systematically study parameters like deflection, energy absorption, stress, strain and deformation behavior and it is in agreement with similar existing researches, Patel *et al.* (2023).

4. Results and discussion

To demonstrate a detailed and comprehensive implementation of the designed and developed model, we present studies on a square plate whose details have been mentioned in Section 3.2. We compute the stresses and strains and examine extensively the role of different strains, the role of different material properties and plate thicknesses.

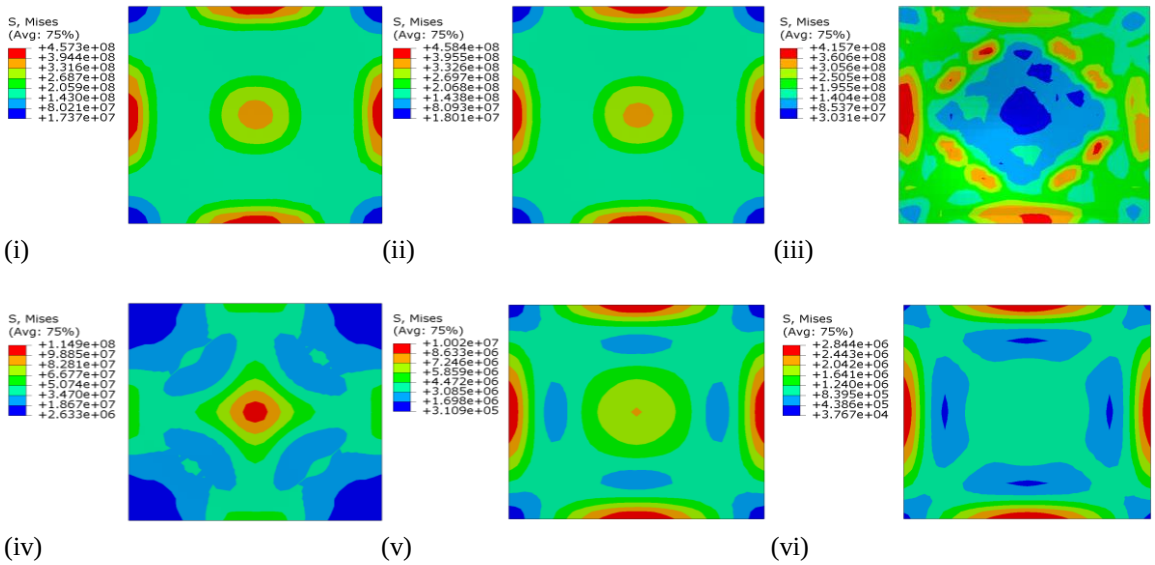

Fig. 5 (a) Von mises stress contours for Case 1 under 1 kg TNT blast at different heights of detonations, i.e., (i) At 0.0 m, (ii) At 0.001 m, (iii) At 0.1 m, (iv) At 0.5 m, (v) At 2 m and (vi) At 3.4 m

We present the results as follows:

- *Case 1:* This case deals with 'mild steel (MS)' plate of 0.03 m thickness under the explosion of 1 kg (Case 1A) and 3 kg (Case 1B) TNT masses, along with different stand-off distances.

- *Case 2:* This case deals with 'mild steel (MS)' plate of 0.04 m thickness under the explosion of 1 kg (Case 2A) and 3 kg (Case 2B) TNT masses, along with different stand-off distances.

- *Case 3:* This case deals with 'e-glass fiber (EGF)' plate of 0.03 m thickness under the explosion of 1 kg (Case 3A) and 3 kg (Case 3B) TNT masses, along with different stand-off distances.

- *Case 4:* This case deals with 'e-glass fiber (EGF)' plate of 0.04 m thickness under the explosion of 1 kg (Case 4A) and 3 kg (Case 4B) TNT masses, along with different stand-off distances.

In each case, we compute Von-Mises stresses, strains, and displacements in the plate.

4.1 Case 1 Detailed results and discussion ('mild steel (MS)' plate, 0.03 m thickness, 1 kg (Case 1A) and 3 kg (Case 1B) TNT masses)

As noted before, herein, we consider the TNT detonations at different heights of: 0.0 m, 0.001 m, 0.1 m, 0.5 m, 2 m, and 3.4 m. For these we compute and show in:

- For 1 kg TNT: Fig. 5(a) - Von mises stress contours, Fig. 6(a) - Maximum principal strain contours, and Fig. 7(a) - Displacement contours. From these results of Figs. 5(a)-7(a), we compute and list in: Table 4(a) - Maximum and minimum stresses, Maximum and minimum strains, and Maximum and minimum displacements.

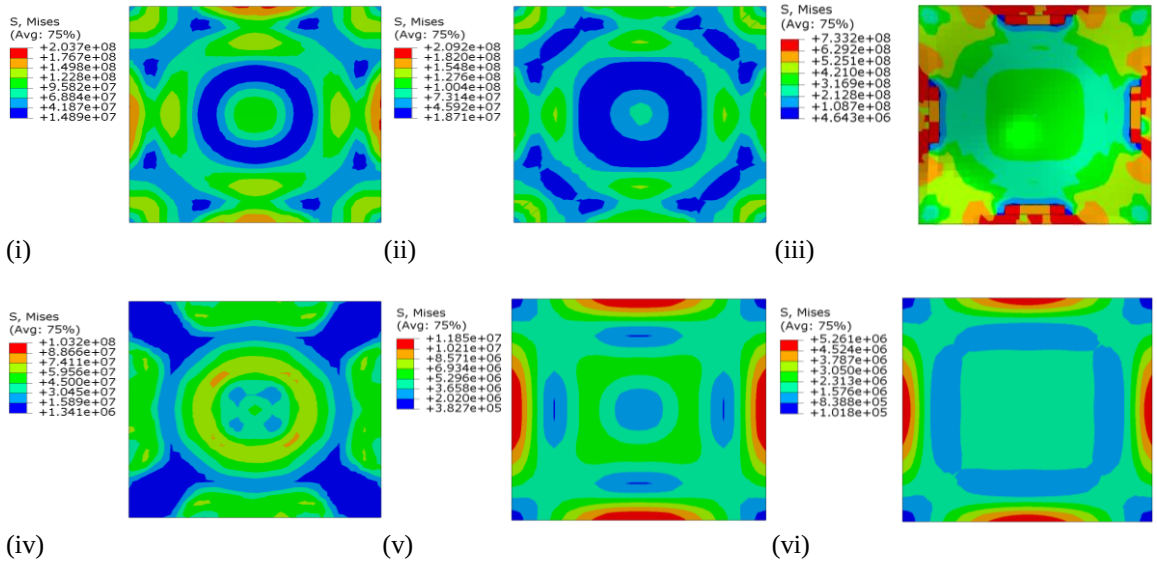

Fig. 5 (b) Von mises stress contours for Case 1 under 3 kg TNT blast at different heights of detonations, i.e., (i) At 0.0 m, (ii) At 0.001 m, (iii) At 0.1 m, (iv) At 0.5 m, (v) At 2 m and (vi) At 3.4 m

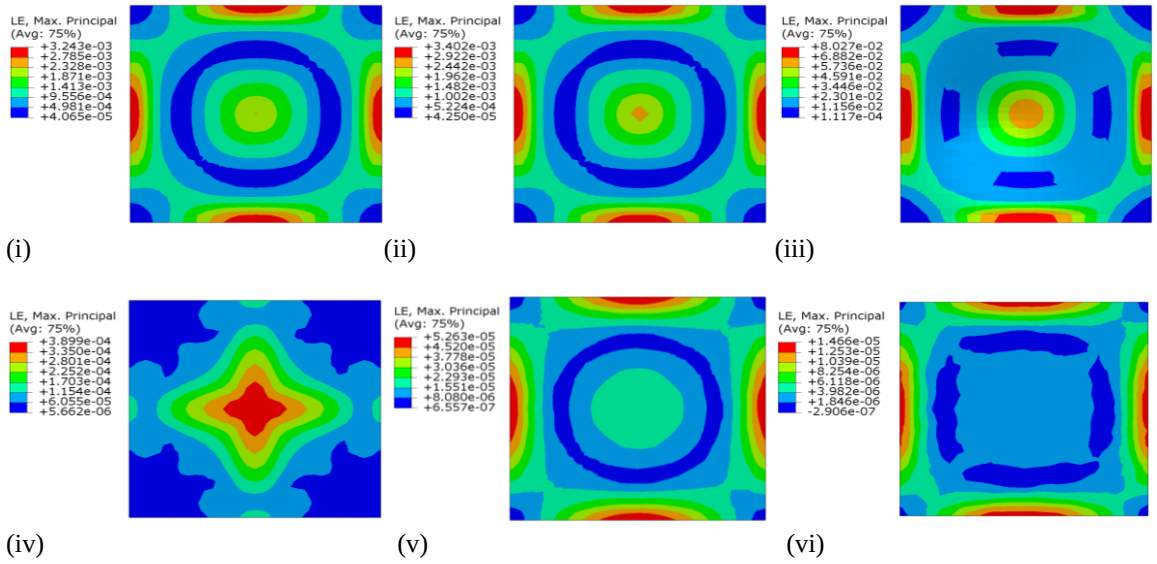

Fig. 6 (a) Maximum principal strain contours for Case 1 under 1 kg TNT blast at different heights of detonations, i.e., (i) At 0.0 m, (ii) At 0.001 m, (iii) At 0.1 m, (iv) At 0.5 m, (v) At 2 m and (vi) At 3.4 m

- For 3 kg TNT: Fig. 5(b) - Von mises stress contours, Fig. 6(b) - Maximum principal strain contours, and Fig. 7(b) - Displacement contours. From these results of Figs. 5(b)-7(b), we compute and list in: Table 4(b) - Maximum and minimum stresses, Maximum and minimum strains, and Maximum and minimum displacements.

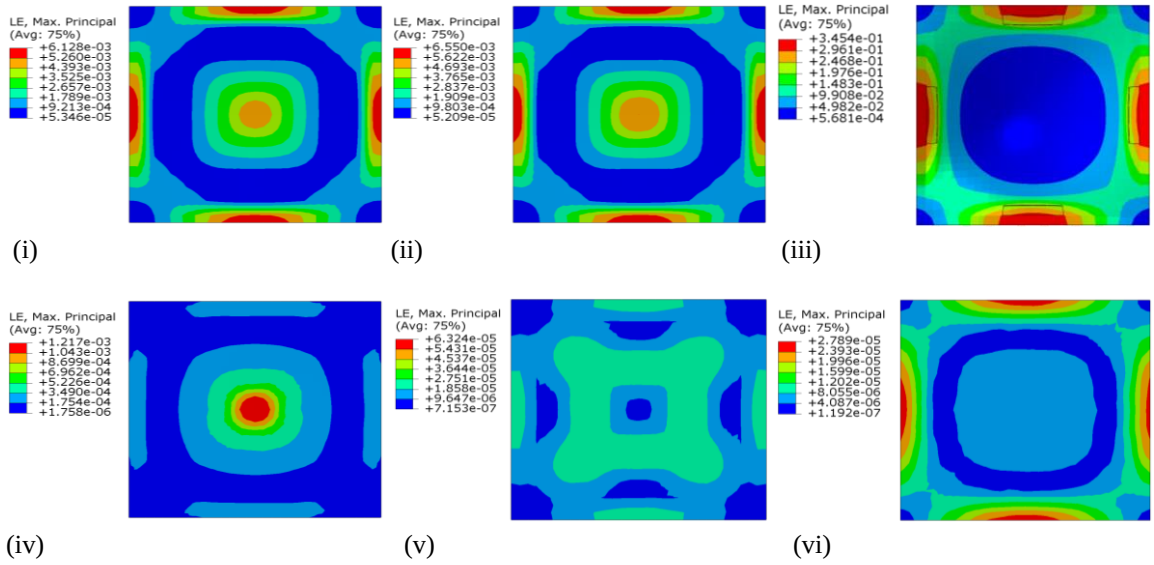

Fig. 6 (b) Maximum principal strain contours for Case 1 under 3 kg TNT blast at different heights of detonations, i.e., (i) At 0.0 m, (ii) At 0.001 m, (iii) At 0.1 m, (iv) At 0.5 m, (v) At 2 m and (vi) At 3.4 m

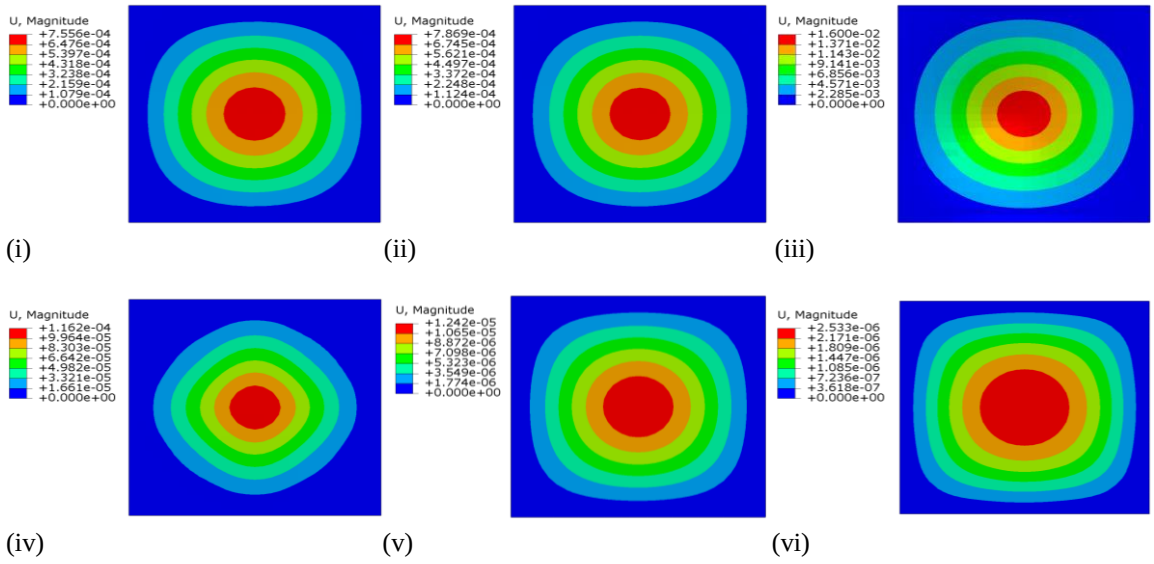

Fig. 7 (a) Displacement contours for Case 1 under 1 kg TNT blast at different heights of detonations, i.e., (i) At 0.0 m, (ii) At 0.001 m, (iii) At 0.1 m, (iv) At 0.5 m, (v) At 2 m and (vi) At 3.4 m

From the results of Fig. 5(a) and Table 4(a), we can note that the Von mises stress (maximum stress) is increasing from 0.0 m explosive height to 0.001 m explosive height and after that it starts decreasing from 0.001 m explosive height to 3.4 m explosive height. This is expected because the impact through explosion primarily propagates forward as a wave that recedes (damped) after a

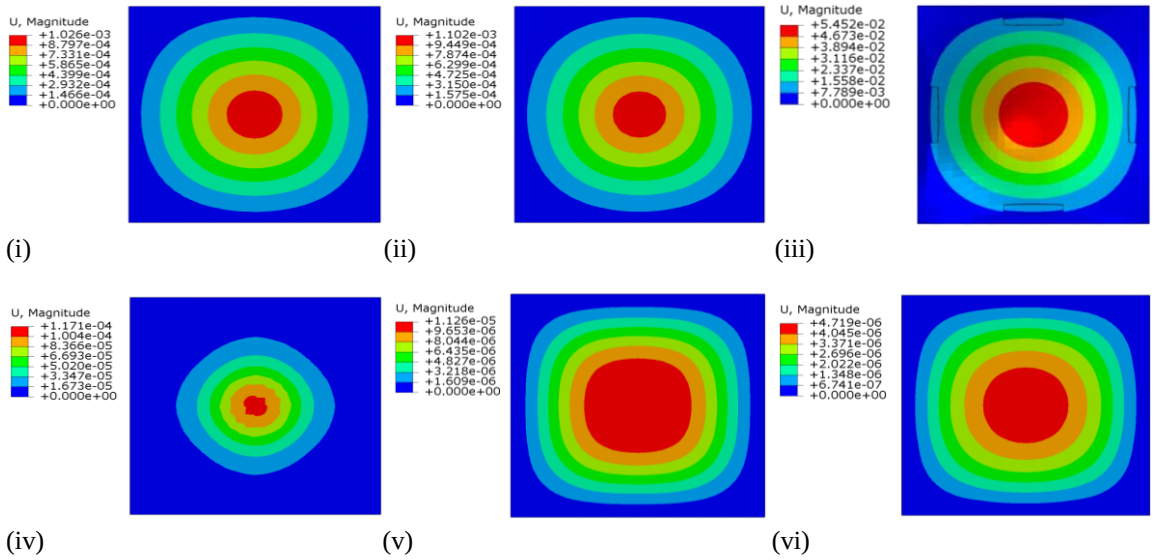

Fig. 7 (b) Displacement contours for Case 1 under 3 kg TNT blast at different heights of detonations, i.e., (i) At 0.0 m, (ii) At 0.001 m, (iii) At 0.1 m, (iv) At 0.5 m, (v) At 2 m and (vi) At 3.4 m

critical distance. After this critical distance the impact through explosion shows no effect and stresses becomes extremely low/insignificant, e.g., after at 3.4 m and afterwards the stresses are very low. Since, this case deals with the mild streel that is highly elastic (with significant plastic range too), and the plate thickness is large, the minimum strains are governed by the EI. Because of this, from the results of Fig. 5(a) and Table 4(a), we can note that the minimum stress increases from 0.0 m to 0.1 m explosive height after that it starts decreasing till 3.4 m explosive height. Because of the properties of elasticity (modulus of elasticity), plasticity and plate thickness, the stresses are correlated with strains. From the results of Fig. 6(a) and Table 4(a), we can note that the maximum strain increases from 0.0 m explosive height to 0.1 m explosive height and after that it starts decreasing from 0.1 m explosive height to 3.4 m explosive height. The minimum strain increases from 0.0 m to 0.1 m explosive height after that it starts decreasing till 3.4 m explosive height. Results of stresses and strains are reflected in the displacement behaviour of the plate and we can note from the results of Fig. 7(a) and Table 4(a) that the maximum displacement increases from 0.0 m explosive height to 0.1 m explosive height and after that it starts decreasing from 0.1 m explosive height to 3.4 m explosive height. As we start at the condition of rest, the minimum displacement is 0 from 0.0 m to 3.4 m explosive height. Even for the 3 kg TNT, the results for 30 mm plate follow similar pattern (with 1 kg TNT) for the mild steel because it has high E, ductility

Table 4 (a) Summary of maximum and minimum stresses, maximum and minimum strains, and maximum and minimum displacements for Case 1A

S. No.	Stress (Pa)		Strain		Displacement (m)	
	Maximum	Minimum	Maximum	Minimum	Maximum	Minimum
Case 1A	4.58E+08	3.77E+04	8.03E-02	-2.90E-07	1.60E-02	0

Table 4 (b) Summary of maximum and minimum stresses, maximum and minimum strains, and maximum and minimum displacements for Case 1B

S. No.	Stress (Pa)		Strain		Displacement (m)	
	Maximum	Minimum	Maximum	Minimum	Maximum	Minimum
Case 1B	7.33E+08	1.02E+05	3.45E-01	1.19E-07	5.45E-02	0

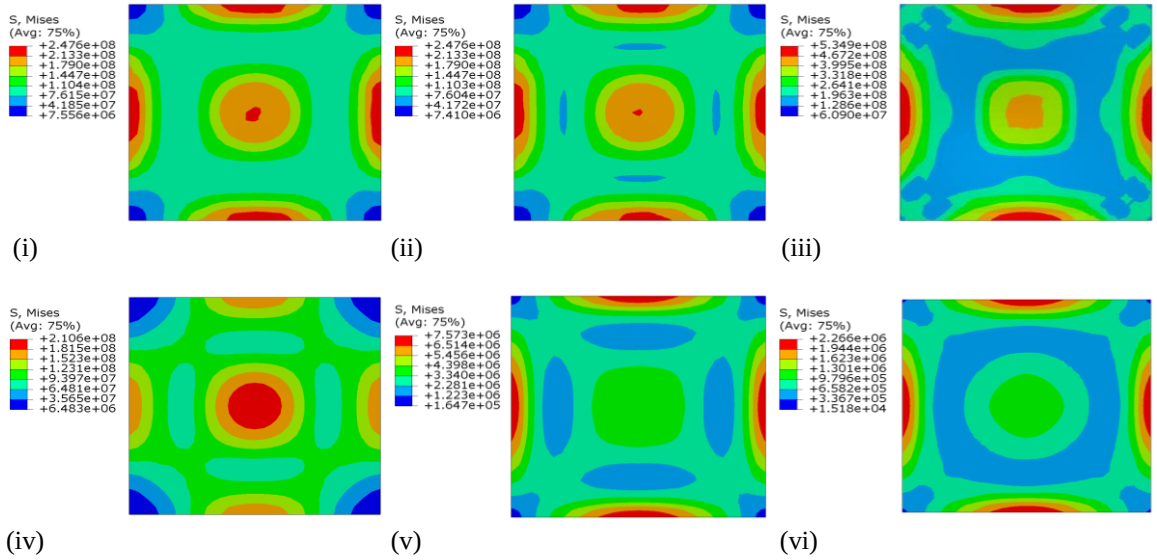

Fig. 8 (a) Von mises stress contours for Case 2 under 1 kg TNT blast at different heights of detonations, i.e., (i) At 0.0 m, (ii) At 0.001 m, (iii) At 0.1 m, (iv) At 0.5 m, (v) At 2 m and (vi) At 3.4 m

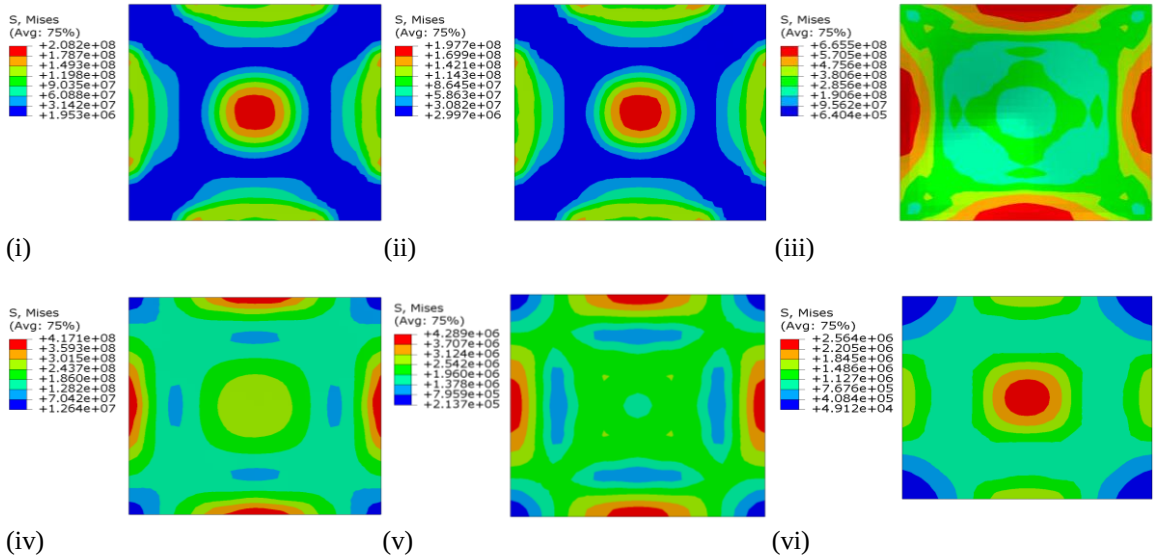

Fig. 8 (b) Von mises stress contours for Case 2 under 3 kg TNT blast at different heights of detonations, i.e., (i) At 0.0 m, (ii) At 0.001 m, (iii) At 0.1 m, (iv) At 0.5 m, (v) At 2 m and (vi) At 3.4 m

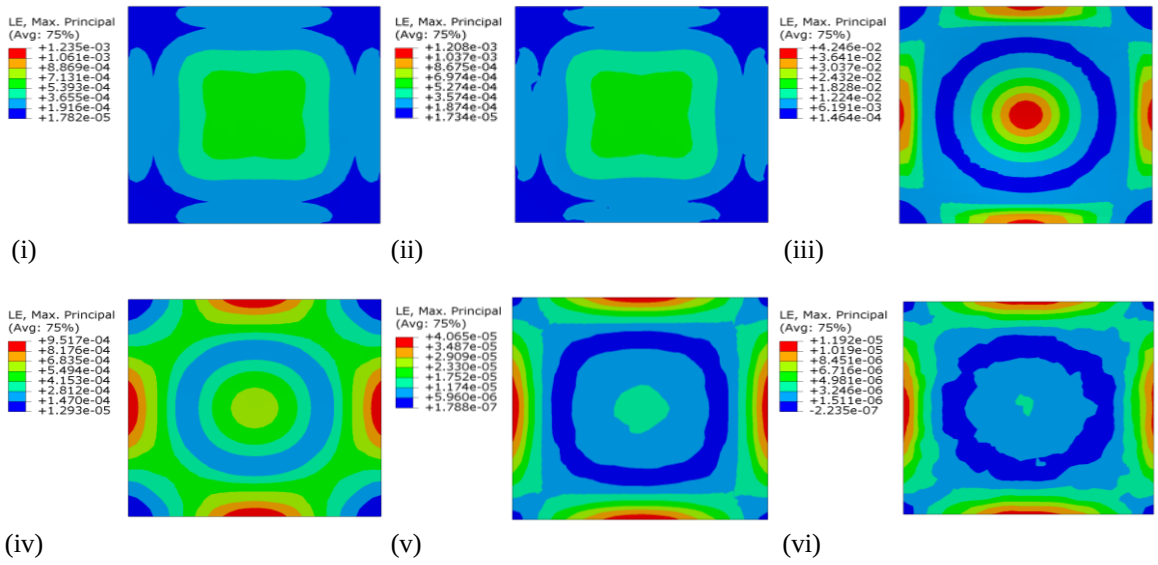

Fig. 9 (a) Maximum principal strain contours for Case 2 under 1 kg TNT blast at different heights of detonations, i.e., (i) At 0.0 m, (ii) At 0.001 m, (iii) At 0.1 m, (iv) At 0.5 m, (v) At 2 m and (vi) At 3.4 m

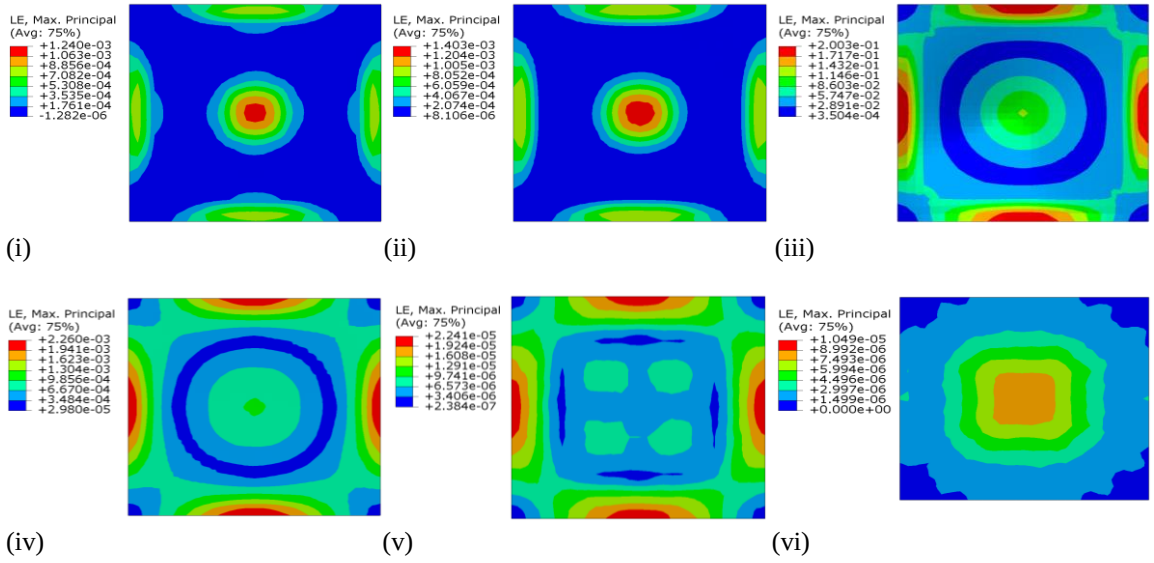

Fig. 9 (b) Maximum principal strain contours for Case 2 under 3 kg TNT blast at different heights of detonations, i.e., (i) At 0.0 m, (ii) At 0.001 m, (iii) At 0.1 m, (iv) At 0.5 m, (v) At 2 m and (vi) At 3.4 m

and equivalent yield strengths in compression and tension. From the results of Fig. 5(b) and Table 3(b), we can note that the Von mises stress (maximum stress) increases from 0.0 m to 0.1 m explosive height and after that it starts decreasing up to 3.4 m explosive height. This is expected

because herein (Case 1B) 3 kg TNT is considered in comparison with the 1 kg TNT in Case 1A and as the total impact energy released with 3 kg TNT is much higher in comparison with 1 kg TNT, the energy propagates over a larger distance and peaks (in terms of amplitude) at a larger distance from the point of impact through explosion. After reaching its peak, it starts reducing as also happens in Case 1A. Since, the peak moves away from the point of impact through explosion, the minimum stresses move closer to the point of impact. So, the minimum stress increases from 0.00 m to 0.001 m explosive height and after that it starts decreasing up to 3.4 m explosive height. Strains and displacements follow similar pattern. As noted before, the impact energy released in Case 1B is higher than Case 1A, and the material is mild steel, in Case 1B maximum and minimum stresses, maximum and minimum strains, and maximum and minimum displacements, are higher in comparison with Case 1A. These results are summarized in Table 4(b). Finally, also we can note that in both Cases 1A and 1B, the maximum stresses are less than the ultimate strength of material and because of this the plate is able to survive and neither a thickness through penetration nor any material failure nor failure through a hole is anticipated herein.

4.2 Case 2 Detailed results and discussion ('mild steel (MS)' plate, 0.04 m thickness, 1 kg (Case 2A) and 3 kg (Case 2B) TNT masses)

As noted before, herein, we consider the TNT detonations at different heights of: 0.0 m, 0.001 m, 0.1 m, 0.5 m, 2 m, and 3.4 m. For these we compute and show in:

- For 1 kg TNT: Fig. 8(a)- Von mises stress contours, Fig. 9(a) - Maximum principal strain contours, and Fig. 10(a) - Displacement contours. From these results of Figs. 8(a)-10(a), we compute and list in: Table 5(a) - Maximum and minimum stresses, Maximum and minimum strains, and Maximum and minimum displacements.
- For 3 kg TNT: Fig. 8(b) - Von mises stress contours, Fig. 9(b) - Maximum principal strain contours, and Fig. 10(b) - Displacement contours. From these results of Figs. 8(b)-10(b), we compute and list in: Table 5(b) - Maximum and minimum stresses, Maximum and minimum strains, and Maximum and minimum displacements.

From the results of Fig. 8(a) and Table 5(a), we can note that the Von mises stress (maximum stress) is increasing from 0.0 m explosive height to 0.001 m explosive height and after that it starts decreasing from 0.001 m explosive height to 3.4 m explosive height. As noted previously, this is expected because the impact through explosion primarily propagates forward as a wave that recedes (damped) after a critical distance. After this critical distance the impact through explosion shows no effect and stresses becomes extremely low/insignificant, e.g., after at 3.4 m and afterwards the stresses are very low. Since, this case deals with the mild streel that is highly elastic (with significant plastic range too), and the plate thickness is large, the minimum strains are governed by the EI. Because of this, from the results of Figs. 8(a)-10(a) and Table 5(a), we can note that the minimum stress increases from 0.0 m to 0.1 m explosive height after that it starts decreasing till 3.4 m explosive height. As noted before, because of the properties of elasticity (modulus of elasticity), plasticity and plate thickness, the stresses are correlated with strains. Previous discussion related to Case 1A is valid here too and the results of maximum strain, minimum strain and displacement follow a similar pattern.

Even for the 3 kg TNT, the results for 30 mm plate follow similar pattern (with 1 kg TNT) for the mild steel because it has high E, ductility and equivalent yield strengths in compression and tension. From the results of Figure 8B and Table 5B, we can note that the Von mises stress (maximum stress) increases from 0.0 m to 0.1 m explosive height and after that it starts decreasing

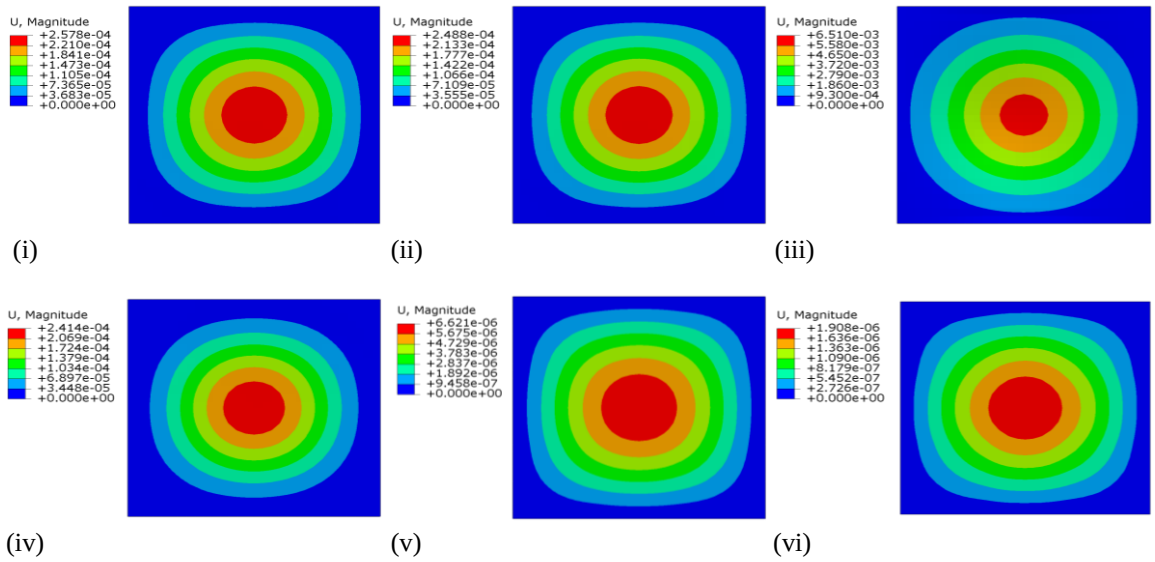

Fig. 10 (a) Displacement contours for Case 2 under 1 kg TNT blast at different heights of detonations, i.e., (i) At 0.0 m, (ii) At 0.001 m, (iii) At 0.1 m, (iv) At 0.5 m, (v) At 2 m, (vi) At 3.4 m

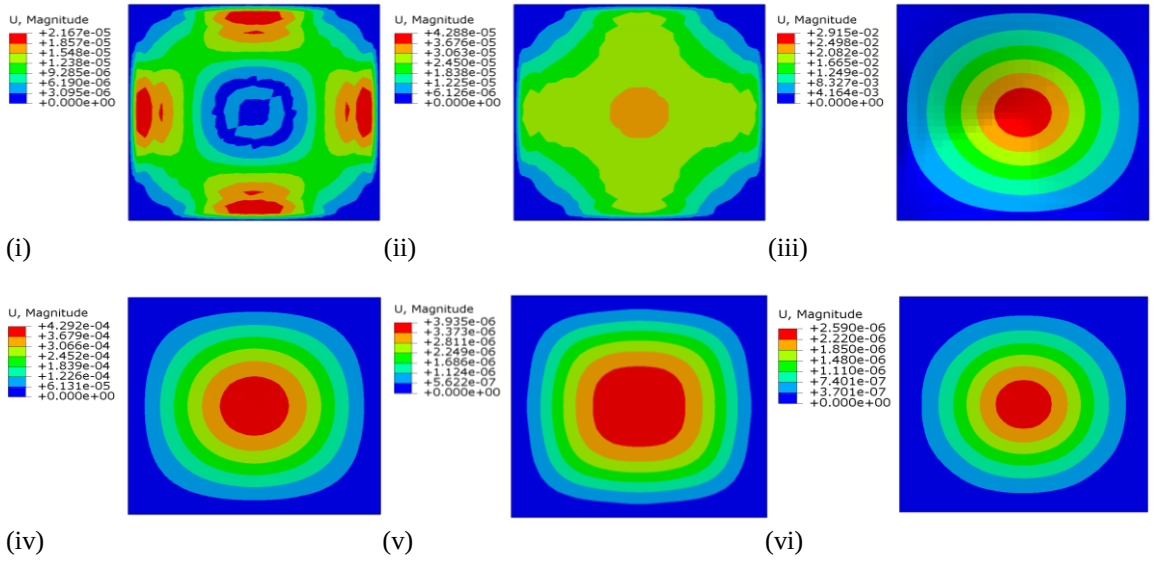

Fig. 10 (b) Displacement contours for Case 2 under 3 kg TNT blast at different heights of detonations, i.e., (i) At 0.0 m, (ii) At 0.001 m, (iii) At 0.1 m, (iv) At 0.5 m, (v) At 2 m and (vi) At 3.4 m

up to 3.4 m explosive height. As discussed previously in Case 1, this is expected because herein (Case 2B) 3 kg TNT is considered in comparison with the 1 kg TNT in Case 2A and as the total impact energy released with 3 kg TNT is much higher in comparison with 1kg TNT, the energy propagates over a larger distance and peaks (in terms of amplitude) at a larger distance from the

point of impact through explosion. Hence, the discussion on Case 1 follows here and is valid too. And, so the minimum stress increases from rom 0.00 m to 0.1 m explosive height and after that it starts decreasing till 3.4 m explosive height. Strains and displacements follow similar pattern. As mentioned before, the impact energy released in Case 2B is higher than Case 2A, and the material is mild steel, in Case 2B maximum and minimum stresses, maximum and minimum strains, and maximum and minimum displacements, are higher in comparison with Case 1A. These results are summarized in Table 5B.

Finally, also we can note that in both Cases 2A and 2B, the maximum stresses are less than the ultimate strength of material and because of this the plate is able to survive and neither a thickness crack through penetration nor any material failure nor failure through a hole, is anticipated herein.

4.3 Case 3 Detailed results and discussion ('e-glass fiber (EGF)' plate, 0.03 m thickness, 1 kg (Case 3A) and 3 kg (Case 3B) TNT masses)

As noted before, herein, we consider the TNT detonations at different heights of: 0.0 m, 0.001 m, 0.1 m, 0.5 m, 2 m, and 3.4 m. For these we compute and show in:

- For 1 kg TNT: Fig. 11(a) - Von mises stress contours, Fig. 12(a) - Maximum principal strain contours, and Fig. 13(a)- Displacement contours. From these results of Figs. 11(a)-13(a), we compute and list in: Table 6(a) - Maximum and minimum stresses, Maximum and minimum strains, and Maximum and minimum displacements.
- For 3 kg TNT: Figure 11B - Von mises stress contours, Fig. 12(b) - Maximum principal strain contours, and Fig. 13(b) - Displacement contours. From these results of Figs. 11(b)-13(b), we compute and list in: Table 6(b) - Maximum and minimum stresses, Maximum and minimum strains, and Maximum and minimum displacements.

From the results of Fig. 11(a) and Table 6(a), we can note that the Von mises stress (maximum stress) is increasing from 0.0 m height to 0.1 m explosive height and it peaks at some distance that is lesser than 0.1 m. This occurrence of high stresses close to 0.1 m distance, results into failure of the plate as a hole is created in the impact through explosion. Once the plate fails (failure through a hole) the stresses starts following a non-linear pattern (i.e., can decrease or increase) depending upon the size of hole. As the hole results into loss of sectional modulus (I) and lower EI further, the stresses normally increase for some distance. But overall these become extremely low because maximum energy is absorbed in the material while failure and after that only little energy will remain to be propagated. We can note here that in comparison with Cases 1 and 2, this case deals with the e-glass fiber that offers high compressive yield strength, low tensile yield strength, low ductility, low elastic range (without any plastic range too), and the plate thickness is large, the EI is not really large in comparison with the mild steel. This low value of EI affects the resulting minimum strains in e-glass fiber. From Table 6A, we can note that the maximum strain increases from 0.00 m to 0.1 m explosive height and after that it starts decreasing from 0.1 m to 3.4 m explosive height. Minimum strains follow the same pattern. We need to mention here that in the failure of plate Case; the stresses, strains and displacement, all peaks, and after peaking out, the computed values do not carry much meaning and lose their importance. As previously, because of the properties of elasticity (modulus of elasticity), yield strength and plate thickness, the stresses are correlated with strains. However, here the E is low in comparison with mild steel, I is same and so overall EI will be lower. This lower EI affects the displacement and strains. And the plate fails because of the Low E. Maximum strain increases from 0.0 m explosive height to 0.1 m explosive height after that it starts decreasing from 0.1 m explosive height to 3.4 m explosive height from the

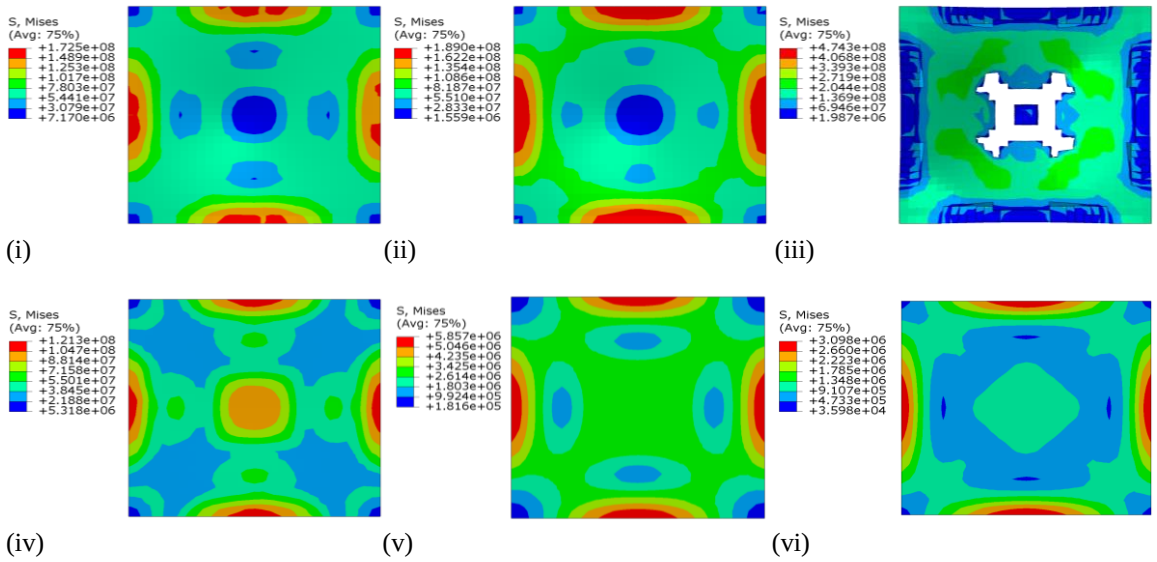

Fig. 11 (a) Von mises stress contours for Case 3 under 1 kg TNT blast at different heights of detonations, i.e., (i) At 0.0 m, (ii) At 0.001 m, (iii) At 0.1 m, (iv) At 0.5 m, (v) At 2 m and (vi) At 3.4 m

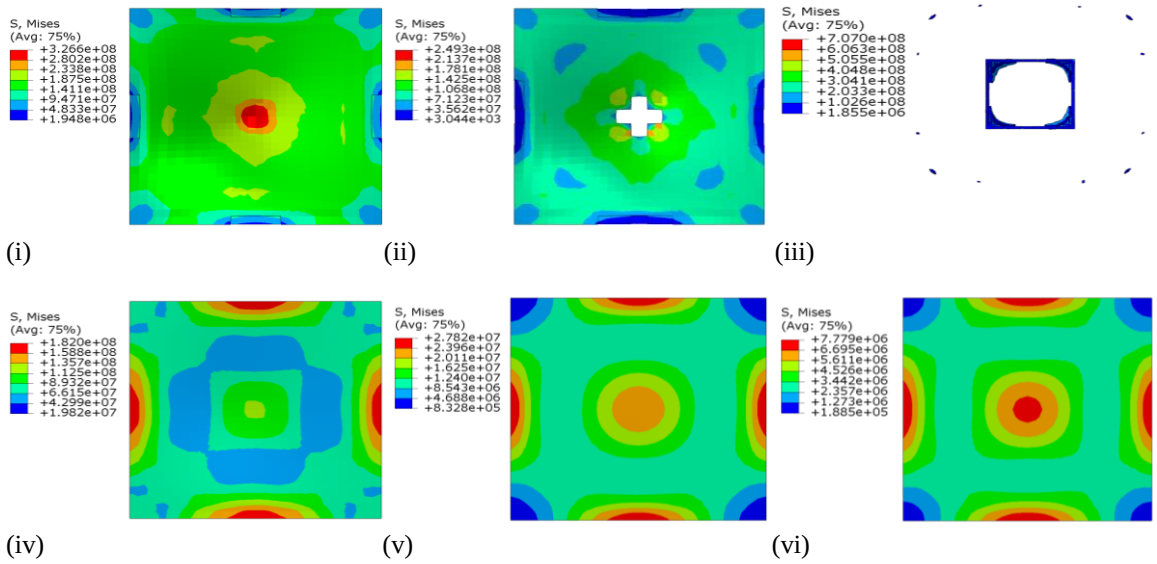

Fig. 11 (b) Von mises stress contours for Case 3 under 3 kg TNT blast at different heights of detonations, i.e., (i) At 0.0 m, (ii) At 0.001 m, (iii) At 0.1 m, (iv) At 0.5 m, (v) At 2 m and (vi) At 3.4 m

plate. Similarly minimum strain also increases from 0.0 m to 0.1 m explosive height and after that it starts decreasing till 3.4 m explosive height. Even for the 3 kg TNT, the results for 30 mm plate follow similar pattern (with 1 kg TNT) for the e-glass fiber plate because it has low density, high compressive yield strength and low E. From the results of Fig. 11(B) and Table 6(b), we can note

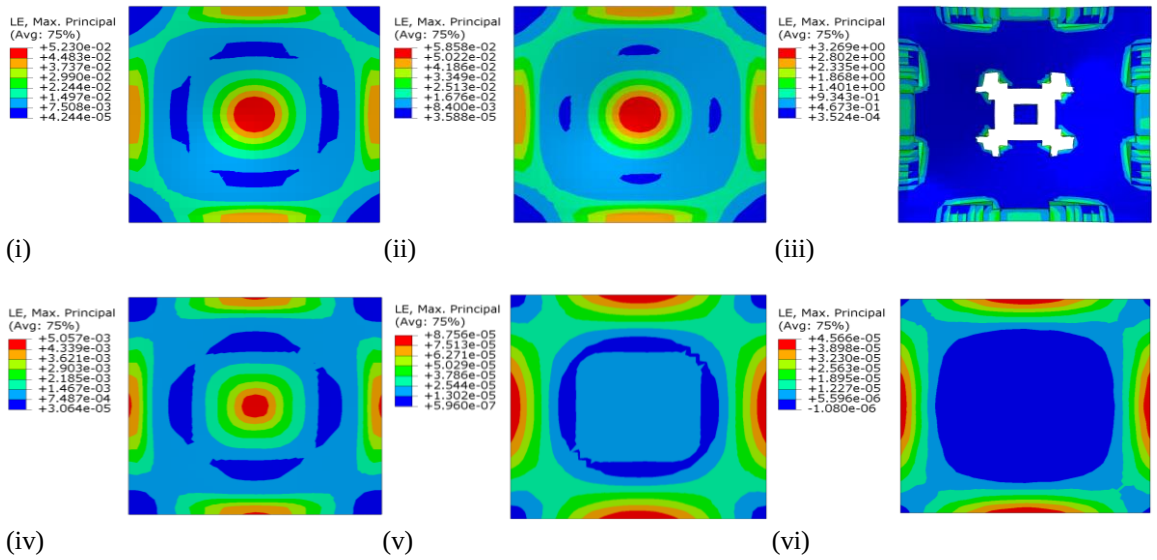

Fig. 12 (a) Maximum principal strain contours for Case 3 under 1 kg TNT blast at different heights of detonations, i.e., (i) At 0.0 m, (ii) At 0.001 m, (iii) At 0.1 m, (iv) At 0.5 m, (v) At 2 m and (vi) At 3.4 m

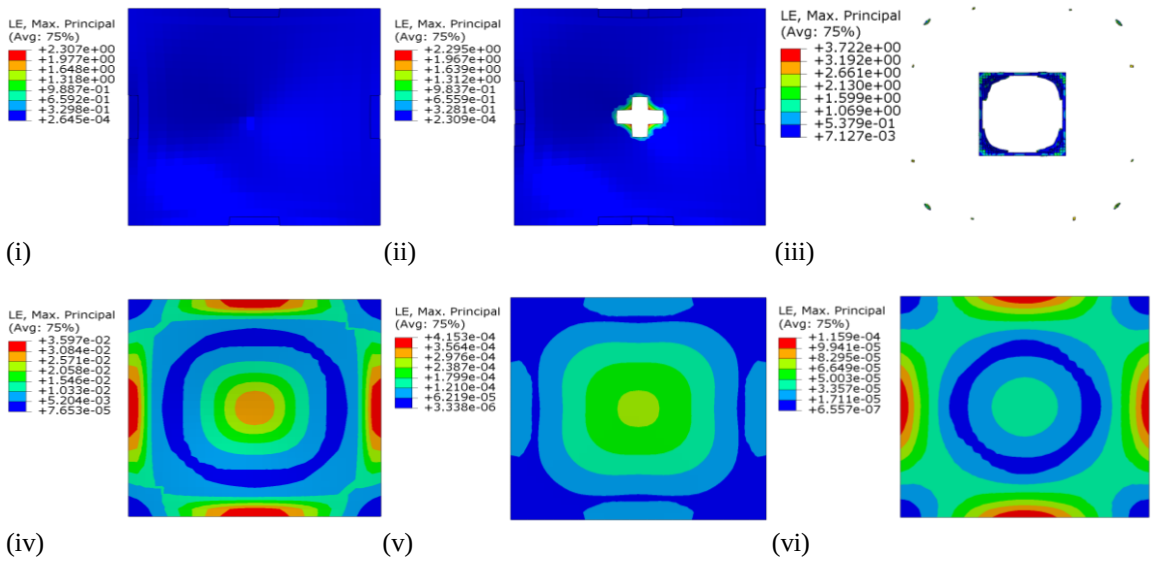

Fig. 12 (b) Maximum principal strain contours for Case 3 under 3 kg TNT blast at different heights of detonations, i.e., (i) At 0.0 m, (ii) At 0.001 m, (iii) At 0.1 m, (iv) At 0.5 m, (v) At 2 m and (vi) At 3.4 m

that the Von mises stress (maximum stress) increases from 0.0 m explosive height to 0.001 m explosive height. This occurrence of high stresses extremely close to the plate at a distance of 0.001 only, results into failure of the plate as a hole is created in the impact through explosion. As noted previously, once the plate fails (failure through a hole) the stresses starts decreasing and

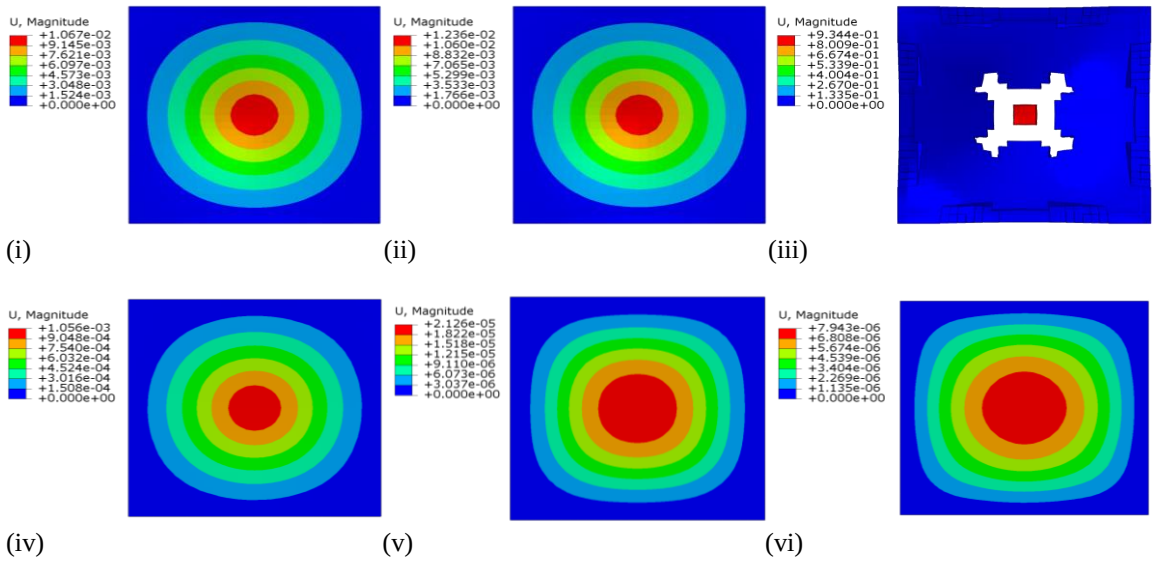

Fig. 13 (a) Displacement contours for Case 3 under 1 kg TNT blast at different heights of detonations, i.e., (i) At 0.0 m, (ii) At 0.001 m, (iii) At 0.1 m, (iv) At 0.5 m, (v) At 2 m and (vi) At 3.4 m

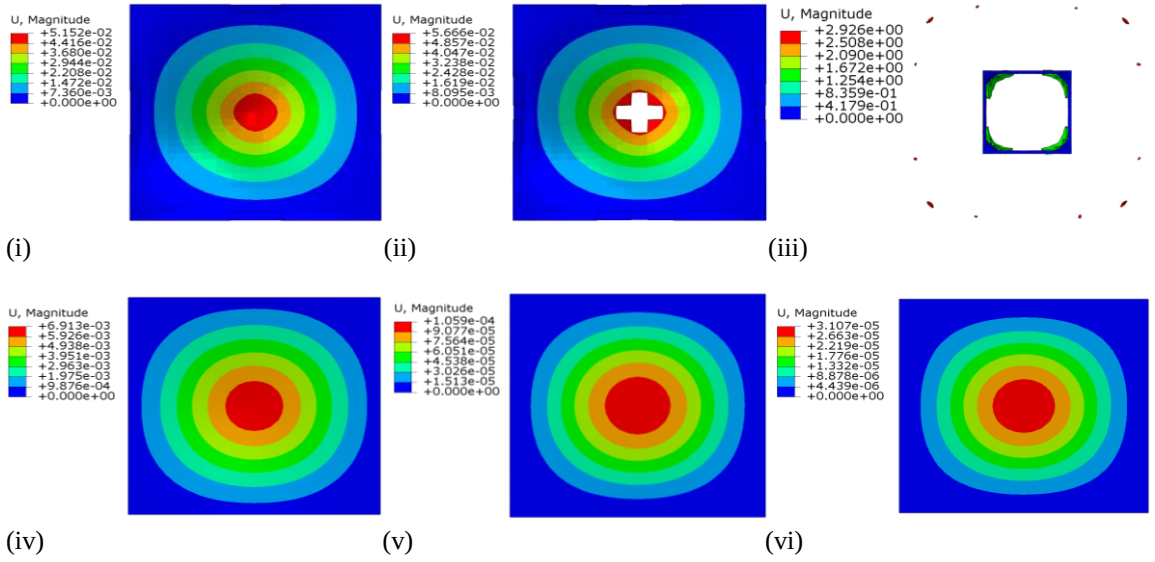

Fig. 13 (b) Displacement contours for Case 3 under 3 kg TNT blast at different heights of detonations, i.e., (i) At 0.0 m, (ii) At 0.001 m, (iii) At 0.1 m, (iv) At 0.5 m, (v) At 2 m and (vi) At 3.4 m

these become extremely low. Herein (Case 3B) 3 kg TNT is considered in comparison with the 1 kg TNT in Case 3A and as the total impact energy released with 3 kg TNT is much higher in comparison with 1kg TNT, hence, the plate fails at much lower explosive height (at 0.001 m) in comparison with the explosive height of 0.1 m in Case 3A. Other discussion points are valid here

Table 5 (a) Summary of maximum and minimum stresses, maximum and minimum strains, and maximum and minimum displacements for Case 2A

S. No.	Stress (Pa)		Strain		Displacement (m)	
	Maximum	Minimum	Maximum	Minimum	Maximum	Minimum
Case 2A	5.35E+08	1.52E+04	4.24E-02	-2.24E-07	6.51E-03	0

Table 5 (b) Summary of maximum and minimum stresses, maximum and minimum strains, and maximum and minimum displacements for Case 2B

S. No.	Stress (Pa)		Strain		Displacement (m)	
	Maximum	Minimum	Maximum	Minimum	Maximum	Minimum
Case 2B	7.33E+08	1.02E+05	3.45E-01	1.19E-07	5.45E-02	0

Table 6 (a) Summary of maximum and minimum stresses, maximum and minimum strains, and maximum and minimum displacements for Case 3A

S. No.	Stress (Pa)		Strain		Displacement (m)	
	Maximum	Minimum	Maximum	Minimum	Maximum	Minimum
Case 3A	4.74E+08	3.60E+04	3.27E+00	-1.08E-06	9.34E-01	0

Table 6 (b) Summary of maximum and minimum stresses, maximum and minimum strains, and maximum and minimum displacements for Case 3B

S. No.	Stress (Pa)		Strain		Displacement (m)	
	Maximum	Minimum	Maximum	Minimum	Maximum	Minimum
Case 3B	7.07E+08	1.89E+05	3.72E+00	6.56E-07	2.93E+00	0

Table 7 (a) Summary of maximum and minimum stresses, maximum and minimum strains, and maximum and minimum displacements for Case 4A

S. No.	Stress (Pa)		Strain		Displacement (m)	
	Maximum	Minimum	Maximum	Minimum	Maximum	Minimum
Case 4A	4.70E+08	2.40E+04	2.64E+00	-7.00E-07	4.63E-02	0

Table 7 (b) Summary of maximum and minimum stresses, maximum and minimum strains, and maximum and minimum displacements for Case 4B

S. No.	Stress (Pa)		Strain		Displacement (m)	
	Maximum	Minimum	Maximum	Minimum	Maximum	Minimum
Case 4B	8.53E+08	1.53E+04	3.60E+00	8.94E-08	1.76E+00	0

too, e.g., properties of e-glass fiber like high compressive yield strength, low tensile yield strength, low ductility, low elastic range (without any plastic range too), and the large plate thickness, etc. From Table 6(b), we can note that the maximum strain increases from 0.0 m to 0.1 m explosive height and after that it starts decreasing from 0.1 m to 3.4 m explosive height. Minimum strains follow the same pattern. As before, we note here too that in the failure of plate Case; the stresses,

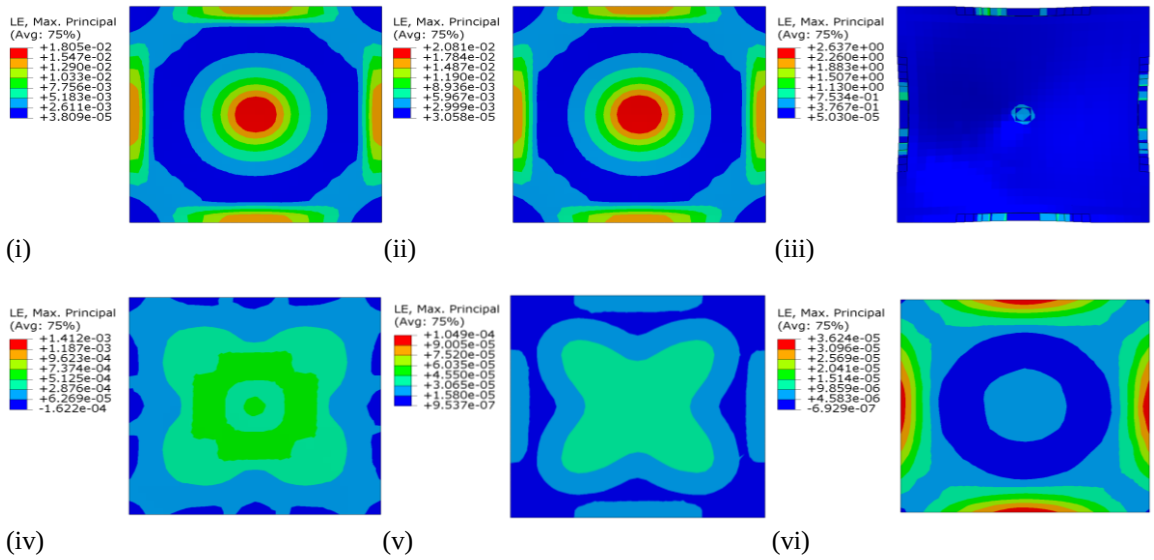

Fig. 14 (a) Von mises stress contours for Case 4 under 1 kg TNT blast at different heights of detonations, i.e., (i) At 0.0 m, (ii) At 0.001 m, (iii) At 0.1 m, (iv) At 0.5 m, (v) At 2 m and (vi) At 3.4 m

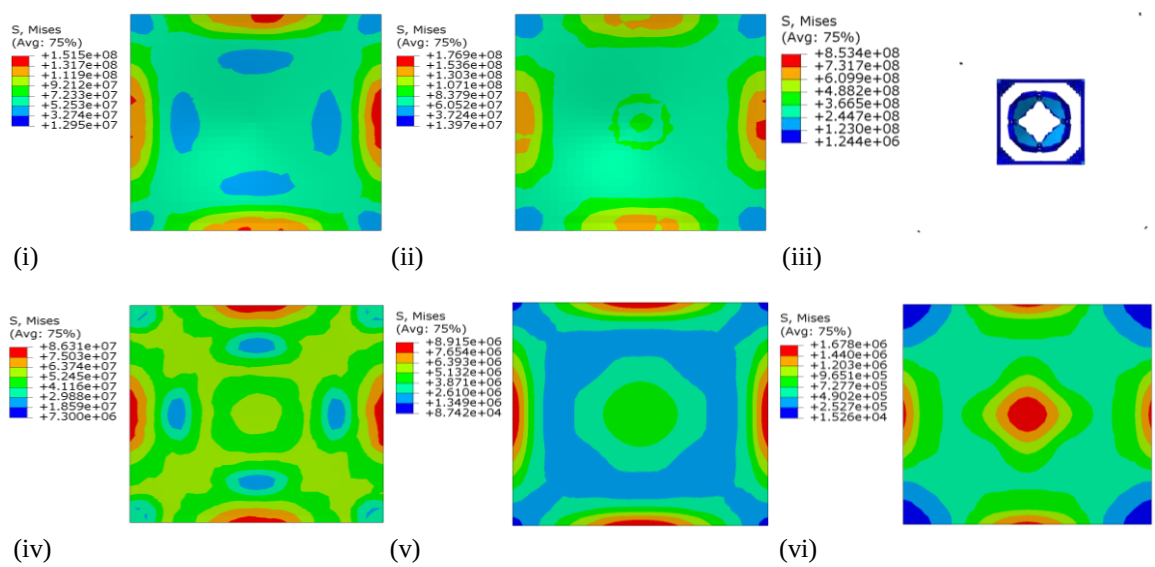

Fig. 14 (b) Von mises stress contours for Case 4 under 3 kg TNT blast at different heights of detonations, i.e., (i) At 0.0 m, (ii) At 0.001 m, (iii) At 0.1 m, (iv) At 0.5 m, (v) At 2 m and (vi) At 3.4 m

strains and displacement, all peaks, and after peaking out, the computed values do not carry much meaning and lose their importance.

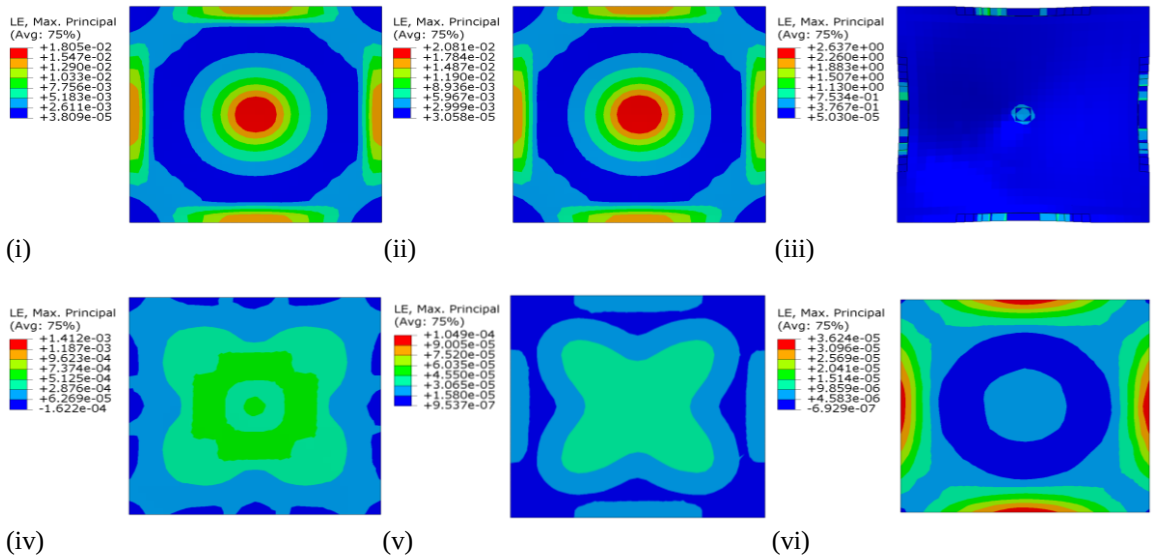

Fig. 15 (a) Maximum principal strain contours for Case 4 under 1 kg TNT blast at different heights of detonations, i.e., (i) At 0.0 m, (ii) At 0.001 m, (iii) At 0.1 m, (iv) At 0.5 m, (v) At 2 m and (vi) At 3.4 m

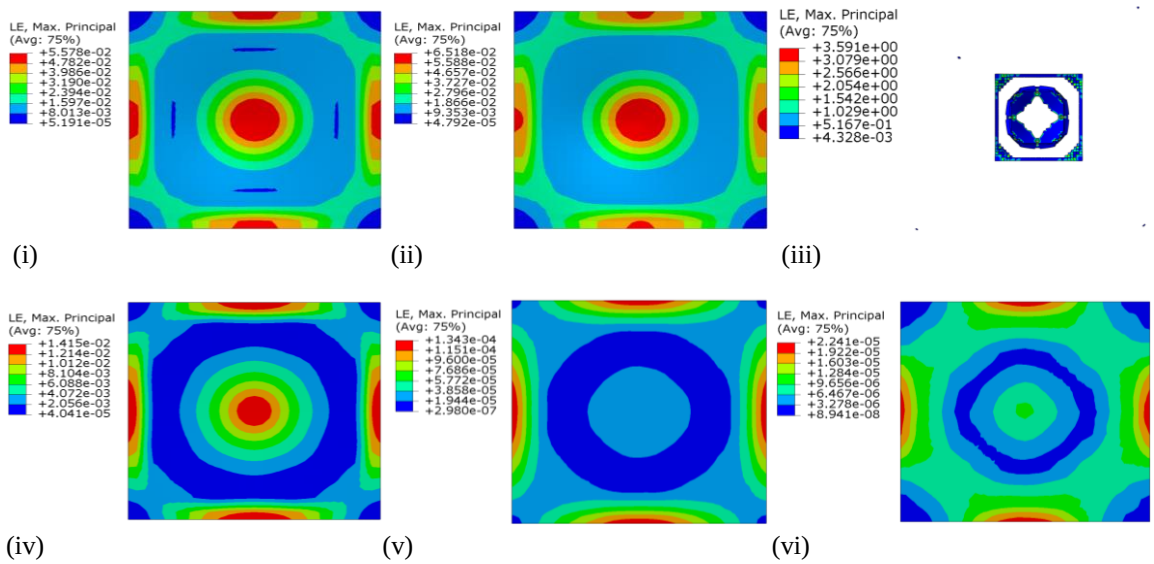

Fig. 15 (b) Maximum principal strain contours for Case 4 under 3 kg TNT blast at different heights of detonations, i.e., (i) At 0.0 m, (ii) At 0.001 m, (iii) At 0.1 m, (iv) At 0.5 m, (v) At 2 m and (vi) At 3.4 m

4.4 Case 4 Detailed results and discussion ('e-glass fiber (EGF)' plate, 0.04 m thickness, 1 kg (Case 4A) and 3 kg (Case 4B) TNT masses)

As noted before, herein, we consider the TNT detonations at different heights of: 0.0 m, 0.001

m, 0.1 m, 0.5 m, 2 m, and 3.4 m. For these we compute and show in:

- For 1 kg TNT: Fig. 14(a) - Von mises stress contours, Fig. 15(a) - Maximum principal strain contours, and Fig. 16(a) - Displacement contours. From these results of Figs. 14(a)-16(a), we compute and list in: Table 7(a)- Maximum and minimum stresses, Maximum and minimum strains, and Maximum and minimum displacements.
- For 3 kg TNT: Fig. 14(b) - Von mises stress contours, Fig. 15(b) - Maximum principal strain contours, and Fig. 16(b) - Displacement contours. From these results of Figs. 14(b)-16(b), we compute and list in: Table 7(b) - Maximum and minimum stresses, Maximum and minimum strains, and Maximum and minimum displacements.

From the results of Fig. 14(a) and Table 7(a), we can note that the Von mises stress (maximum stress) is increasing from 0.0 m to 0.1 m explosive height and after that it starts decreasing up to 3.4 m explosive height. This occurrence of high stresses close to 0.1 m distance, is expected as explained previously but does not result into failure of the plate because the plate thickness here is larger than in Cases 3A and 3B. Large thickness results in to higher I, and higher EI, and because of the higher EI, resulting stresses get lower. Because of the low stresses, the plate failure is averted. From Table 6(a), we can note that the maximum strain is increasing from 0.0 m to 0.1 m explosive height and after that it starts decreasing from 0.1 m to 3.4 m explosive height. Similarly minimum strain is also increasing from 0.0 m to 0.5 m explosive height after that it's started decreasing till 3.4 m explosive height.

For the 3 kg TNT, the results for 40 mm plate follow a slightly different pattern (with 1 kg TNT) for the e-glass fiber plate because although it still has low density, high compressive yield strength and low E, the impact energy through explosion is larger here. From the results of Fig. 14(b) and Table 7(b), we can note that the Von mises stress (maximum stress) increases from 0.0 m explosive height to 0.1 m explosive height. This occurrence of high stresses close to the plate at a distance of 0.1 m, results into failure of the plate as a hole is created in the impact through explosion. As mentioned before, once the plate fails (failure through a hole) the stresses starts decreasing and these become extremely low. Herein (Case 4B) 3 kg TNT is considered in comparison with the 1 kg TNT in Case 4A and as the total impact energy released with 3kg TNT is much higher in comparison with 1kg TNT, hence, the plate fails here while it does not in Case 4A. Other discussion points are valid here too, e.g., properties of e-glass fiber like high compressive yield strength, low tensile yield strength, low ductility, low elastic range (without any plastic range too), and the large plate thickness, etc. From Table 7(b), we can note that the maximum strain increases from 0.0 m to 0.1 m explosive height and after that it starts decreasing from 0.1 m to 3.4 m explosive height. Minimum strains follow roughly the same pattern. Also increasing from 0.0 m to 0.1 m explosive height after that it's started decreasing till 3.4 m explosive height. As before, we note here too that in the failure of plate Case; the stresses, strains and displacement, all peaks, and after peaking out, the computed values do not carry much meaning and lose their importance.

Finally, also we can note that in Cases 3A, 3B, and 4B, the maximum stresses are higher than the yield strength of material and because of this the plate fails. Only in Case 4A the plate is able to survive because of its high thickness and lower mass of TNT explosion (1 kg). This shows that the use of e-glass fiber in the applications where impact through explosion is significant, is not really advisable.

5. Overall summary of the results and discussion

Overall, from Figs. 17 (a) and 17(b), we note and summarize:

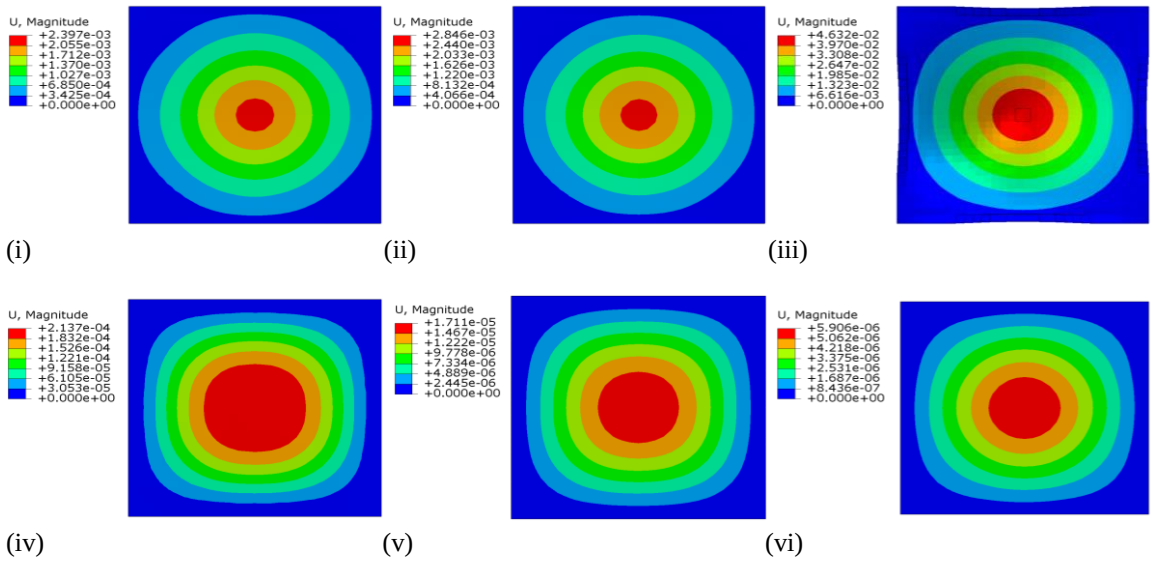

Fig. 16 (a) Displacement contours for Case 4 under 1 kg TNT blast at different heights of detonations, i.e., (i) At 0.0 m, (ii) At 0.001 m, (iii) At 0.1 m, (iv) At 0.5 m, (v) At 2 m and (vi) At 3.4 m

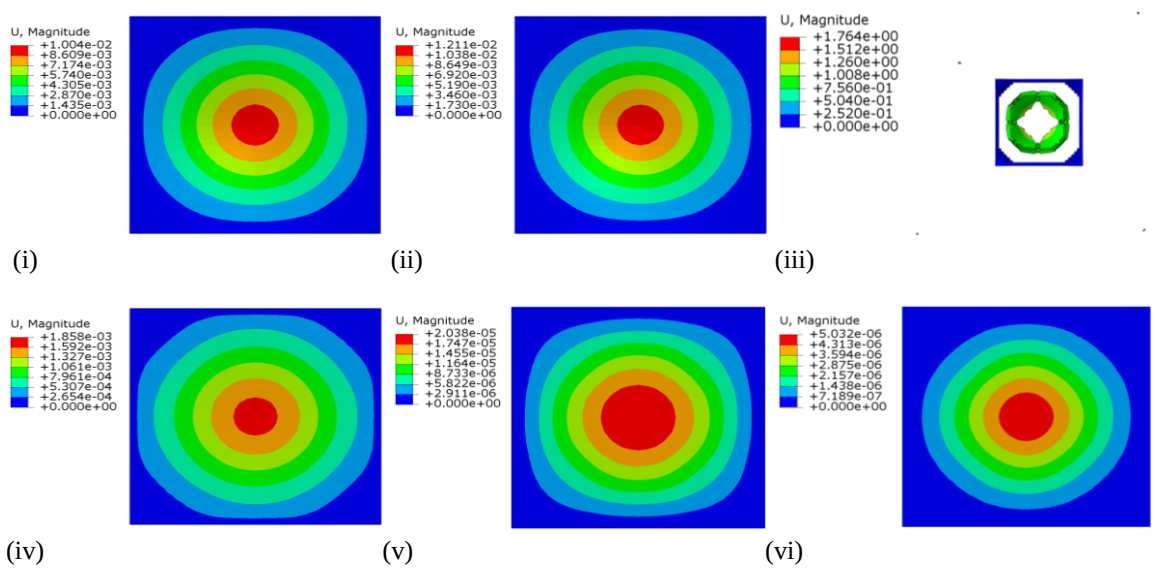

Fig. 16 (b) Displacement contours for Case 4 under 3 kg TNT blast at different heights of detonations, i.e., (i) At 0.0 m, (ii) At 0.001 m, (iii) At 0.1 m, (iv) At 0.5 m, (v) At 2 m and (vi) At 3.4 m

- Maximum stress is increasing with increasing stand-off distance of explosive (TNT) from the material plate in positive z direction and we observe that the stress is maximum at '***0.1***' m stand-off distance, and after that it starts decreasing up to '***3.4***' m stand-distance.

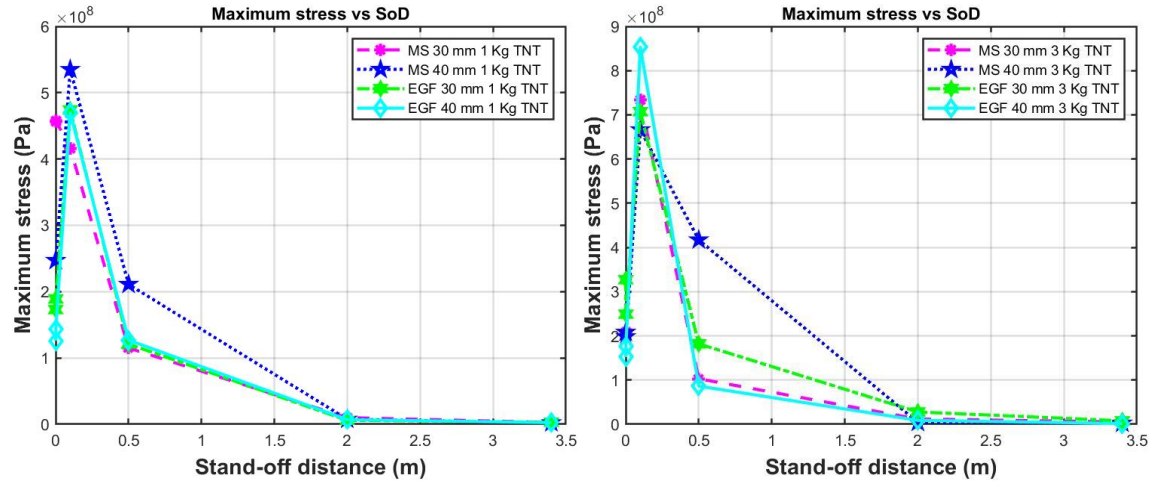

(A) (B)

Fig. 17 (a) Variation of the maximum stress versus stand-off distance for the 30 mm and 40 mm for the mild steel and e-glass fiber plates, at different heights of 1 kg TNT detonations; and (b) - Variation of the maximum stress versus stand-off distance for the 30 mm and 40 mm for the mild steel and e-glass fiber plates, at different heights of 3 kg TNT detonations. Heights are: 0.0, 0.001, 0.1, 0.5, 2 and 3.4, all in m

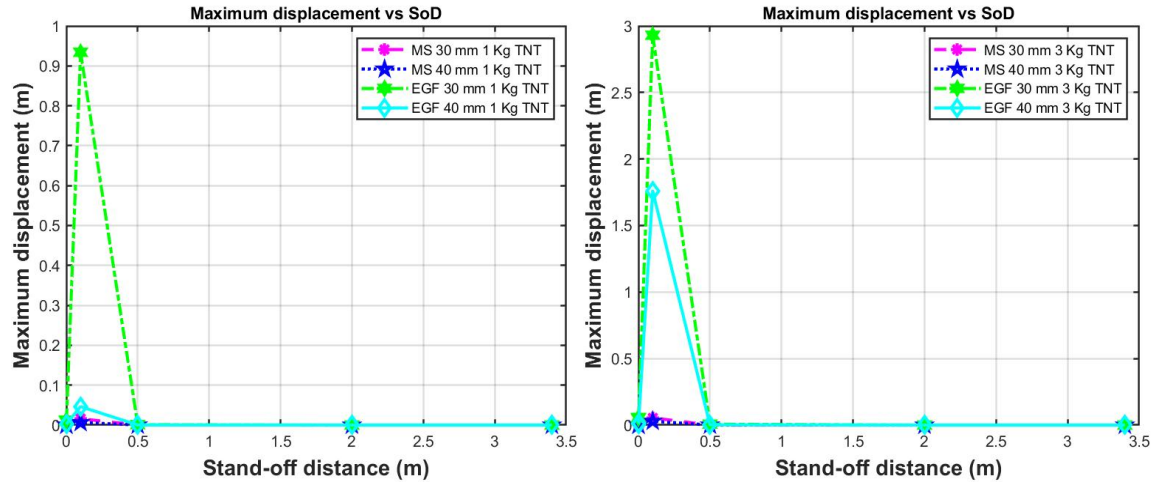

(A) (B)

Fig. 18 (a) Variation of the maximum displacement versus stand-off distance for the 30 mm and 40 mm for the mild steel and e-glass fiber plates, at different heights of 1 kg TNT detonations; and (b) Variation of the maximum displacement versus stand-off distance for the 30 mm and 40 mm for the mild steel and e-glass fiber plates, at different heights of 3 kg TNT detonations. Heights are: 0.0, 0.001, 0.1, 0.5, 2 and 3.4, all in m

- Similarly, from Figs. 18 (a) and 18(b), we note that the maximum displacement is increasing with increasing stand-off distance of explosive (TNT) from the material plate in positive z direction.

- From these results, we observe that the displacement is maximum at '***0.1***' m stand-off distance, after that it starts decreasing up to '***3.4***' m stand-of distance.

- In the 'e-glass' fiber case for 30 mm thickness plate with 1 kg TNT and 3 kg TNT; and 40 mm thickness plate with 3 kg TNT, the plate show clear breaking and failure.

Hence, from the design and application point of view a distance close to the plate is critically important and increasing thicknesses without proper selection of a material is not an effective and efficient design approach.

6. Conclusions

We presented the design and development of a 'Finite Element Analysis (FEA)' based model incorporating temperature dependent material properties for impact analysis of blasts on underwater vehicles. Our model has been motivated by the idea of the incorporation of temperature dependent material properties in explosion studies for the design and development of new age shield engineering designs. We presented extensive results that are likely to become an important key towards bench marking and showed and analysed the effect of explosion on square plates of different materials and distribution of stresses, strains and displacements after explosion/impact, etc. Our presented FEA based model has been governed by the basic numerical analysis, finite element analysis and thermal/material science and our implementation has been in ABAQUS^{*TM} and Matlab^{**TM} software solution systems through the development/incorporation/inclusion/integration of subroutines. Our focus has been on large deformation finite element analysis, and we used the Jones-Wilkins-Lee (JWL) equation of state, Johnson Cook parameters, along with temperature dependent material properties. Overall, based upon the presented results and their analyses, we can state:

- ***(A)*** If the plate thickness is low then composite plates fail earlier then steel but if sufficient thickness is provided in that case as thickness increases maximum stresses also start decreasing. However, it is not the case with steel. This is mainly because of the low E for composites.

- ***(B)*** Maximum stresses are low for the composites because composites have very high yield strength (in compression), especially in compression. However composites fail with even a lower amount of TNT blast because their total energy absorption capacity is low. Because of their lower E and ultimate strength (in tension), they do not allow large plastic deformation, are not ductile and show sudden failure.

- ***(C)*** Maximum displacement is much higher for the composites because composite materials have low E in comparison with steel. Hence in the case of e-glass fiber maximum displacements are high, although the maximum stresses are low. From the material science perspective, the maximum stresses are governed by the yield strength and the maximum displacement and strains are governed by E.

However, we also note here that we have not attempted a detailed analysis of exploring the direct relationships among different material properties, amount of the TNT blast, and failure. Our future work will go in this direction and currently this is under investigation.

Acknowledgements

This research was supported by the internal research grants of IIT Madras, Chennai, India and the first author was supported by the MoE, GoI, India scholarship scheme (reference number: OE19D020).

Trademark and copyrights

*Trademark and copyright with Dassault Systèmes SE, France. **Trademark and copyright with MathWorks, USA.

References

Aune, V., Fagerholt, E., Hauge, K.O., Langseth, M. and Børvik, T. (2016), "Experimental study on the response of thin aluminium and steel plates subjected to airblast loading", *Int. J. Impact Eng*., **90**, 106-121. https://doi.org/10.1016/j.ijimpeng.2015.11.017.

Beshara, F.B.A. (1994), "Modelling of blast loading on aboveground structures - I: General phenomenology and external blast", *Comput. Struct.*, **51**(5), 585-596. https://doi.org/10.1016/0045-7949(94)90066-3.

Cimpoeru, S.J., Ritzel, D.V. and Brett, J.M. (2017), Physics of explosive loading of structures. *In Explosion Blast Response of Composites. Woodhead Publishing,* USA, 1-22.

Cole, R.H. and Weller, R. (1948), "Underwater explosions", *Phys. Today*, **1**(6), 35-35.

Conrath, E.J. (1999), Structural design for physical security: State of the practice, *ASCE Publications*.

Cranz, K.J. (1925), Lehrbuch der ballistik (Vol. 1). *Рипол Классик.*

Das, S,K., Mandal, K,K. and Niyogi, A,G. (2022), "A finite element based approach to observe hydrodynamic pressure in reservoir adjacent to concrete gravity dam", *Ocean Syst. Eng*., **12**(4), 385-402. https://doi.org/10.12989/ose.2022.12.4.385.

Dharmasena, K.P., Wadley, H.N., Xue, Z. and Hutchinson, J.W. (2008), "Mechanical response of metallic honeycomb sandwich panel structures to high-intensity dynamic loading", *Int. J. Impact Eng.*, **35**(9), 1063-1074. https://doi.org/10.1016/j.ijimpeng.2007.06.008.

Elek, P.M., Dzingalasević, V.V., Jaramaz, S.S. and Micković, D.M. (2015), "Determination of detonation products equation of state from cylinder test: Analytical model and numerical analysis", *Therm. Sci.*, **19**(1), 35-48.

Fordham, S. (2013), High Explosives and Propellants, Elsevier, Amsterdam.

Fu, T., Zhang, M., Zheng, Q., Zhou, D., Sun, X. and Wang, X. (2021), "Scaling the response of armor steel subjected to blast loading", *Int. J. Impact Eng.*, **153**, 103863. https://doi.org/10.1016/j.ijimpeng.2021.103863.

Gan, L., Zong, Z., Chen, Z., Wu, T., Lin, J. and Li, M. (2023), "Differences in responses of square steel plates exposed to blast loads generated by cubic and spherical explosives", *Thin-Wall. Struct*., **182**, 110332. https://doi.org/10.1016/j.tws.2022.110332.

Giam, A., Toh, W. and Tan, V.B.C. (2020), "Numerical review of Jones–Wilkins–Lee parameters for trinitrotoluene explosive in free-air blast", *J. Appl. Mech*., **87**(5), 051008.

Hamdoon, M., Zamani, N. and Das, S. (2011), "FEA of the blast loading effect on ships hull", *Ocean Syst. Eng.*, **1**(3), 223-239. https://doi.org/10.12989/ose.2011.1.3.223.

Hopkinson, B. (1915), British ordnance board minutes 13565, The National Archives, Kew, UK, 11.

Iqbal, M.A., Senthil, K., Bhargava, P. and Gupta, N.K. (2015), "The characterization and ballistic evaluation of mild steel", *Int. J. Impact Eng.*, **78**, 98-113. https://doi.org/10.1016/j.ijimpeng.2014.12.006.

Johnson, G.R. and Cook, W.H. (1985), "Fracture characteristics of three metals subjected to various strains,

strain rates, temperatures and pressures", *Eng. Fract. Mech.*, **21**(1), 31-48. https://doi.org/10.1016/0013-7944(85)90052-9.

Kim, B.W., Hong, S.Y., Sung, H.G. and Hong, S.W. (2015), "Comparison of simplified model and FEM model in coupled analysis of floating wind turbine", *Ocean Syst. Eng.*, **5**(3), 221-243. https://doi.org/10.12989/ose.2015.5.3.221.

Kim, J.H.J., Yi, N.H., Kim, S.B., Choi, J.K. and Park, J.C (2009), "Experiment study on blast loading response of FRP-retrofitted RC slab structures", *Proceedings of the Asia-Pacific Conference on FRP in Structures.*

Kinney, G.F. and Graham, K.J. (2013), Explosive shocks in air. *Springer Science & Business Media*.

Kumar, R. and Patel, S. (2021), "Failure analysis on octagonal honeycomb sandwich panel under air blast loading", *Materials Today: Proceedings*, **46**, 9667-9672. https://doi.org/10.1016/j.matpr.2020.07.525.

Li, Y., Wu, W., Zhu, H., Wu, Z. and Du, Z. (2017), "The influence of different pre-formed holes on the dynamic response of square plates under air-blast loading", *Eng. Fail. Anal.*, **78**, 122-133. https://doi.org/10.1016/j.engfailanal.2017.03.002.

Longère, P., Geffroy-Grèze, A.G., Leblé, B. and Dragon, A. (2013), "Ship structure steel plate failure under near-field air-blast loading: Numerical simulations vs experiment", *Int. J. Impact Eng.*, **62**, 88-98. https://doi.org/10.1016/j.ijimpeng.2013.06.009.

Markose, A. and Rao, C.L. (2017), "Mechanical response of V shaped plates under blast loading", *Thin-Wall. Struct.*, **115**, 12-20. https://doi.org/10.1016/j.tws.2017.02.002.

Mays, G. and Smith, P.D. (Eds.). (1995), Blast effects on buildings: Design of buildings to optimize resistance to blast loading, *Thomas Telford*.

Mlakar, P.F. and Barker, D. (2010), Blast phenomena. Handbook for blast resistant design of buildings, *John Wiley and Sons*.

Mohamed, M.N. (2023), "Improving the blast resistance of sandwich structures by tailoring honeycomb core through varying cell size and vertex-derivative approach", *Forces in Mech.*, **13**, 100247. https://doi.org/10.1016/j.finmec.2023.100247.

Mouritz, A.P. (2019), "Advances in understanding the response of fibre-based polymer composites to shock waves and explosive blasts", *Compos. Part A: Appl. Sci. Manufact.*, **125**, 105502. https://doi.org/10.1016/j.compositesa.2019.105502.

Mubarok, M.A.H., Muttaqie, T., Prabowo, A.R., Sohn, J.M., Surojo, E. and Imaduddin, F. (2022a), "Effects of geometrical variations on the performance of hull plate structures under blast load: A study using nonlinear fea", *Procedia Struct. Integrity*, **41**, 282-289. https://doi.org/10.1016/j.prostr.2022.05.033.

Mubarok, M.A.H., Prabowo, A.R., Muttaqie, T. and Muhayat, N. (2022b), "Dynamic structural assessment of blast wall designs on military-based vehicle using explicit finite element approach", *Math. Problem. Eng.*, **2022**(1), 5883404. https://doi.org/10.1155/2022/5883404.

Nurick, G.N. and Martin, J.B. (1989), "Deformation of thin plates subjected to impulsive loading - a review: Part I: Theoretical considerations", *Int. J. Impact Eng.*, **8**(2), 159-170. https://doi.org/10.1016/0734-743X(89)90014-6.

Nurick, G.N. and Martin, J.B. (1989), "Deformation of thin plates subjected to impulsive loading - a review part II: experimental studies", *Int. J. Impact Eng.*, **8**(2), 171-186. https://doi.org/10.1016/0734-743X(89)90015-8.

Patel, M., Patel, S. and Ahmad, S. (2023), "Blast analysis of efficient honeycomb sandwich structures with CFRP/Steel FML skins", *Int. J. Impact Eng.*, **178**, 104609. https://doi.org/10.1016/j.ijimpeng.2023.104609.

Patel, M. and Patel, S. (2024), "Dynamic behavior analysis of steel, aluminum, and composite plates under extreme air blast loadings", *Mech. Adv. Mater. Struct.*, 1-17. https://doi.org/10.1080/15376494.2024.2427933.

Prabowo, A.R. and Bae, D.M. (2019), "Environmental risk of maritime territory subjected to accidental phenomena: Correlation of oil spill and ship grounding in the Exxon Valdez's case", *Results in Eng.*, **4**, 100035. https://doi.org/10.1016/j.rineng.2019.100035.

Rajendran, R. and Lee, J.M. (2009), "Blast loaded plates", *Mar. Struct.*, **22**(2), 99-127.

https://doi.org/10.1016/j.marstruc.2008.04.001.
Remennikov, A.M. (2003), "A review of methods for predicting bomb blast effects on buildings", *J. Battlefield Technol.*, **6**(3), 5-10.
Sachs, R.G. (1944), Dependence of blast on ambient pressure and temperature, *BRL-466 Ballistic Research Laboratory*, Aberdeen, Maryland.
Safari, K.H., Zamani, J., Khalili, S.M.R. and Jalili, S. (2011), "Experimental, theoretical, and numerical studies on the response of square plates subjected to blast loading", *J. Strain Anal. Eng. Design*, **46**(8), 805-816. https://doi.org/10.1177/0309324711416183.
Shi, Y., Hao, H. and Li, Z.X. (2007), "Numerical simulation of blast wave interaction with structure columns", *Shock Waves*, **17**, 113-133. https://doi.org/10.1007/s00193-007-0099-5.
Shin, Y.S. (2011), "Advances in ship survivability against underwater explosions", *Ocean Syst. Eng.*, **1**(2), 111-119. https://doi.org/10.12989/ose.2011.1.2.111.
Shubham, Yerramalli, C.S., Sumant, C., Prusty, R.K. and Ray, B.C. (2022), "Finite element modelling and experimentation of plain weave glass/epoxy composites under high strain-rate compression loading for estimation of Johnson-Cook model parameters", *Int. J. Impact Eng.*, **167**, 104262. https://doi.org/10.1016/j.ijimpeng.2022.104262.
Smaradhana, D.F., Prabowo, A.R. and Ganda, A.N.F. (2021), "Exploring the potential of graphene materials in marine and shipping industries - A technical review for prospective application on ship operation and material-structure aspects", *J. Ocean Eng. Sci.*, **6**(3), 299-316. https://doi.org/10.1016/j.joes.2021.02.004.
Uddin, N. (Ed.). (2010), Blast protection of civil infrastructures and vehicles using composites, *Elsevier,* New York, USA.
Ullah, A., Ahmad, F., Jang, H. W., Kim, S.W. and Hong, J.W. (2017), "Review of analytical and empirical estimations for incident blast pressure", *KSCE J. Civil Eng*., **21**(6), 2211-2225. https://doi.org/10.1007/s12205-016-1386-4.
UNODA (2011), Formulae for ammunition management IATG 01.80, *United Nations Office for Disarmament Affairs (UNODA)*, New York, USA.
Xu, S.L., Wu, P., Zhou, F., Jiang, X., Chen, B.K. and Li, Q.H. (2020), "A dynamic constitutive model of ultra high toughness cementitious composites", *J. Zhejiang University – Science A*, **21**(12), 939-960. https://doi.org/10.1631/jzus.A1900599.
Yadav, S., Singhal, S., Jasra, Y. and Saxena, R.K. (2020), "Determination of Johnson-Cook material model for weldment of mild steel", *Materials Today: Proceedings*, **28**, 1801-1808. https://doi.org/10.1016/j.matpr.2020.05.213.

MK

Nomenclature

AUV Autonomous underwater vehicle,
ROV Remotely operated vehicle,
CONWEP Conventional weapons effects,
FEA Finite element analysis,
IED Improvised explosive devices,
JWL Jones-Wilkins-Lee,
MS Mild steel,
EGF E-glass fiber,
PCa = Reflected excess pressure,
P = Instantaneous overpressure,
P_P = Peak overpressure,
P_{atm} = Atmospheric pressure,
P_N = Negative pressure,
t_a = Arrival time,
t_{d^+} = Positive duration,
t_d = Negative duration,
t = Time,
λ = Time decay constant,
K = Explosive material constant,
W = Weight,
I = Imparted impulse,
m = Explosive mass,
R = Stand-off distance,
P_s = Shock wave overpressure,
P_i = Incident overpressure,
P_r = Reflected overpressure,
$\bar{\sigma}$ = Yield stress at nonzero strain rate,
$\bar{\varepsilon}^p_{eq}$ = Equivalent plastic strain rate,
$\dot{\varepsilon}_0$ = Reference strain rate,
$\sigma^0\left(\bar{\varepsilon}^p_{eq}, T\right)$ = Static yield stress,
$R\left(\bar{\varepsilon}^p_{eq}\right)$ = Ratio of the yield stress at nonzero strain rate to the static yield stress,
A_v, B_v, n_v, C_v, and m_v = Material parameters as defined in Eq. (10),
T = Material temperature (in degree Kelvin),
T_m = Melting temperature of the material,
T_r = Room temperature,
T_t = Transition temperature,
ρ = Density,
E = Young's modulus of elasticity,
v = Poisson's ratio,
σ_{YA} = Yield stress,
B = Strain hardening constant,

n = Strain hardening coefficiant
C = Strain rate hardening,
m_t = Thermal softening constant,
$D_1\ D_2\ D_3\ D_4\ and\ D_5$ = Different fracture strain constants,
D = Damage variable,
Δ_ε = Equivalent plastic strain,
ε^f = Equivalent strain required to fracture,
σ_m = Average normal stresses,
$\bar{\sigma}_v$ = Von-Mises equivalent stress,
P_a = Applied air pressure,
V_0 = Initial relative volume,
V = Relative volume,
E_o = Initial internal energy density,
C_0–C_6 = Coefficients of the polynomial equation,
$A_j,\ B_j,\ R_1,\ R_2$, and ω = Material constants in JWL state equation as defined in Eq. (15),
P_d = Detonation pressure,
E_m = Internal energy per unit mass,
ρ_o = Density of the unreacted explosive material, and
ρ_d = Density of the reacted detonation products.